CHALMERS
UNIVERSITY OF TECHNOLOGY

Microstructural characterization of cobalt chromium (ASTM F75) cubes produced by EBM technique

Influence of carbon and nitrogen content as well as hot isostatic pressing

By

MANDEEP CHAUHAN

Diploma work No. 198/2017
Master's thesis in **Materials Engineering**

Performed at: **Department of Industrial and Materials Science**
Chalmers University of Technology, SE – 412 96 Gothenburg

Supervisor: Dr. Fouzi Bahbou
Arcam EBM AB
Mölndal, Sweden

Supervisor & Examiner: Prof. Uta Klement
Division of Materials & Manufacture
Chalmers University of Technology

Microstructural characterization of cobalt-chromium (ASTM F75) cubes produced by EBM technique
Influence of carbon and nitrogen content as well as heat treatment
MANDEEP CHAUHAN

Diploma work no xx/2017
Department of Industrial and Materials Science
Chalmers University of Technology
SE-412 96 Gothenburg
Sweden
Telephone + 46 (0)31-772 1000

Cover:
[Columnar grains parallel to the build direction for Co-28Cr-6Mo-0.05C-0.05N in as-built condition]

Printed by Chalmers Reproservice
Gothenburg, Sweden 2017

Microstructural characterization of cobalt-chromium (ASTM F75) cubes produced by EBM technique
Influence of carbon and nitrogen content as well as heat treatment

MANDEEP CHAUHAN
Department of Industrial and Materials Science
Chalmers University of Technology

Abstract

Cobalt-chromium based alloys have been widely used to make biomedical implants for hip and knee joints. The alloy enables to manufacturing metal on metal bearing implants which have increased life and minimum wear debris generated. They have excellent corrosion resistance, wear resistance, high stiffness and high mechanical strength properties. In the past, the alloy implants have been manufactured by investment casting method. However, dental casting implants have been reported to have fractured occasionally on small plastic deformation. In recent years, additive manufacturing by electron beam melting (EBM) technique has been used to manufacture complex design implants with short lead times and minimum post machining.

The alloy consists of two primary phases: a high temperature γ-face centered cubic (γ-fcc) phase which shows high elongation and ultimate tensile strength, other is low temperature ε-hexagonal close packed (ε-hcp) phase which shows low elongation and brittle fracture on straining. Carbon (max. 0.35 wt. %) and nitrogen (max. 0.25 wt. %) are two important trace elements added to increase mechanical strength, elongation and wear resistance of the alloy. They inhibit ε-hcp to γ-fcc phase transformation and provide solid solution and precipitation strengthening. However, increased concentration of precipitates in the form of carbides and nitrides have reported to decrease tensile elongation and strength.

Researchers have concentrated their efforts to find the correct alloy composition and heat treatment to stabilize γ-fcc phase matrix and increase strength for casting and hot forging process. However, little work has been done to optimize alloy composition for EBM technique. With the EBM technique, the alloy is reported to give gassing of carbon and nitrogen compounds that erode the cathode and it requires expensive post heat treatment to increase ductility. It was important to understand the effect of carbon and nitrogen content on microstructure and on corresponding mechanical properties for cobalt-chromium alloy parts manufactured by EBM technique. This thesis investigates the microstructural characteristics of the cubes with varying carbon and nitrogen content under as-built and hot isostatic pressing conditions. The microstructures were evaluated using optical microscopy, scanning electron microscopy including electron back scattered diffraction analysis, and X-ray diffraction. The obtained microstructures are then compared with mechanical tensile test data.

Keywords: Cobalt chromium alloy, EBM, hot isostatic pressing, carbon and nitrogen content, microstructural evaluation, phase analysis, tensile test

Acknowledgements

I would like to thank my supervisor at Arcam EBM AB, Dr. Fouzi Bahbou for providing the opportunity to work on this interesting master thesis topic and for all the material samples. I would also take the opportunity to thank my supervisor and examiner Prof. Uta Klement for constant support and discussion sessions during complete thesis. And for giving access to all the laboratory facilities at the department of industrial and materials science, Chalmers University.

At last, special thanks to research engineers Eric Tam and Yiming Yao for introductory sessions to the laboratory equipments. Thanks to all PhD students of the department for their help and guidance.

Contents

Abbreviations

AM: Additive manufacturing
C: Carbon
Co: Cobalt
Cr: Chromium
CCM: Cobalt-chromium-molybdenum alloy
CCM-C: Cobalt-chromium-molybdenum alloy with carbon
CCM-CN: Cobalt-chromium-molybdenum alloy with carbon and nitrogen
EBM: Electron beam melting
EBSD: Electron back scattered diffraction
Fcc: Face centred cubic
Hcp: Hexagonal close packed
HIP: Hot isostatic pressing
Mo: Molybdenum
Ni: Nickel
N: Nitrogen
OM: Optical microscopy
SEM: Scanning electron microscope
SFE: Stacking fault energy
SF: Stacking fault
SIMT: Strain induced martensitic transformation
SLM: Selective laser melting
UTS: Ultimate tensile strength
XRD: X-ray diffraction
YS: Yield strength

List of figures

List of tables

Introduction

Arcam EBM AB currently develops an electron beam machining (EBM) process for cobalt-chromium molybdenum (CCM) alloy, Co-28Cr-6Mo. The alloy composition and mechanical property requirements are provided in the ASTM F75 standard. The material is commonly used for making orthopaedic implants such as knee and hip joints. The strength of CCM alloy is strongly linked to the material's microstructure, which in turn depends on the chemical composition and the material's thermal history.

Problem statement

Arcam needs to build knowledge of how carbon and nitrogen content and heat treatment control microstructure and consequently the mechanical properties of EBM manufactured CCM alloy parts.

Optimization of carbon (C) and nitrogen (N) content is very important. According to the old powder specifications, C content is 0.22 wt.% and N content is 0.15wt.%. The combination provides very good wear and corrosion resistance but requires expensive and complex heat treatment in two steps to dissolve the carbides in the material. For commercial success, it is important that the heat treatment of CCM be eliminated or simplified.

Secondly, during the EBM processing of CCM alloy, gassing of carbon and nitrogen compounds takes place in the vacuum chamber. These gases erode the ceriumhexaboride cathode in the gun of Q10 machine which reduces the cathode life. The cathode is expensive.

In additive manufacturing (AM) of metal products, potential users approach the technology in two ways:
1) There are some customers who desire to use the metal product without post processing and for these people, as-built properties have a direct impact on acceptance of the AM technology. Their biggest interest in AM is its part and production flexibility which enables them to make customized products in reduced time.
2) There are some customers for whom the as-built properties do not matter much because they will eventually go for post processing like changing phase fraction, grain structure, removing cracks or pores or perform traditional machining like grinding and/or polishing. Their biggest interest in AM is its material and resource efficiency and part flexibility. It is important to note that as-built microstructure is still important for post processing to achieve desired results.

Customers of Arcam utilizing cobalt-chromium powder for additive manufacturing by EBM technology are inclined to manufacture metal products that can be used in as-built condition without the use of extensive post heat treatment procedures. Extensive amount of research has been done to optimize the CCM alloy composition especially C and N content manufactured using the traditional casting and hot forging process. However, not much research on microstructural characterization of EBM fabricated CCM alloy has been published. Effort has been made in this master thesis to characterize microstructure of as-built and HIPed EBM-fabricated solid CCM alloy samples.

Limitations

The microstructural characterization results of this thesis are limited to cubical specimens which are printed close to the build plate. The tensile test specimens were printed along with cubical

specimens and the whole build time was more than 30 hours. The results may vary for cubical specimens printed far from build plate or with lower build times.

Theoretical background

According to the ASTM standard [1], AM can be defined as "process of joining materials to make objects from 3D model data, usually layer upon layer, as opposed to subtractive manufacturing methodologies". It is more commonly known as 3D (three-dimensional) printing, or rapid manufacturing or rapid prototyping. Unlike machining and stamping processes that fabricate parts by removing materials from a metal block, AM creates the final shape by adding material [2].

In principle, it works by consolidating feedstock into dense parts. The feedstock comprises of either powder, sheets or wire and the densification can be achieved by either melting or solid-state joining [3].

Additive manufacturing was first developed 30 years ago by researchers in Austin, Texas when they selectively melted layers of polymer using laser [3]. The laser was then used to selectively melt metal and over the years, tremendous development in metal AM techniques and processes has happened. What started as first '3D printed' metal prototype using selective laser sintering (SLS) in 1990, is now developed using selective laser melting (SLM) in which complete melting of the metal powder is achieved [3].

AM provides various benefits to the manufacturing industry and society in general [4][5]. They are:

- *Material efficiency*: Since AM produces parts layer by layer, it efficiently utilizes the raw material. Contrary, large amount of material had to be removed in conventional subtractive manufacturing.
- *Resource efficiency*: AM directly transfers the computerized 3D model into a finished product without the need for fixtures and cutting tools. Combining this with design flexibility, manufactures can optimize design to achieve lean production and eliminating waste.
- *Part flexibility*: Parts that were manufactured previously by welding various sub parts can now be manufactured in a single part. Design innovation over the years has also made it possible to build a single part with varying mechanical properties (flexible in one corner and stiff in another corner).
- *Production flexibility*: Inherent design flexibility means that production of complex monolithic geometries involving little or no joining operations can be easily achieved as demanded by customer. This is because now the quality depends on the process rather than on operator skills and since AM machines do not require costly setups, it is economical for small batch production. This is a big advantage in eliminating production bottlenecks and producing single pieces.

Since the first development of AM technology, the research and industry has seen registration of various licenses and patents in the AM field throughout US and Europe. However, usage and market are heavily controlled by license and patent holders which has indirectly kept the prices of the manufactured part high [3]. Figure 1 shows a general timeline of introduction of important AM technology.

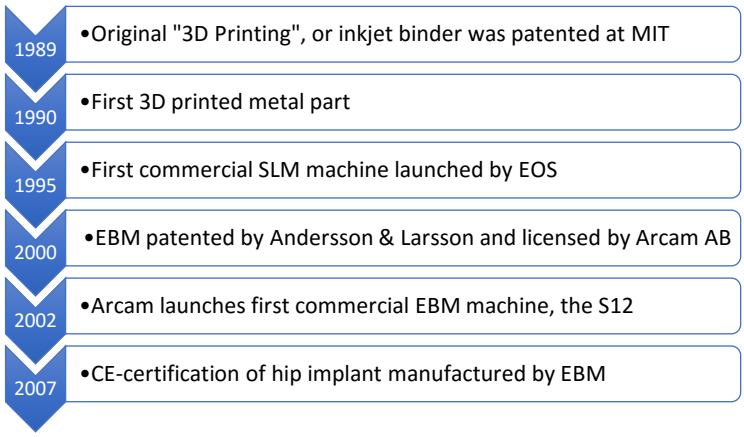

Figure 1 AM timeline

Classification of technologies

According to ASTM F42 Committee on Additive Manufacturing, there are four metal AM standard categories which can be used to classify various AM machines [6]. They are:

1. Powder Bed Fusion
    a. Selective laser melting (SLM)
    b. Electron beam melting (EBM)
2. Direct energy deposition
    a. Laser vs. E-beam
    b. Wire fed vs. powder fed
3. Binder jetting
    a. Infiltration
    b. Consolidation
4. Sheet lamination
    a. Ultrasonic additive manufacturing

Powder-bed fusion

Powder bed fusion works on the principle of selectively melting layer by layer metal powder using either electron beam (in EBM machines) or laser beam (in SLM machines). The fundamental difference between the two machine setups lies in the type of focused energy source used. While the EBM technique employs a high-powered scanning electron beam, SLM technique utilizes laser beam. SLM technique uses a system of mirror lenses to scan the powder bed, operates in an inert environment with nitrogen or argon filling and at around room temperature. EBM technique uses a system of magnetic lenses to scan the powder bed, operates under vacuum environment and sintering of the powder bed layer results in increased operating temperature (600-1100°C).

EBM-system

EBM machines have been commercially manufactured by Arcam EBM AB, Sweden since 2002. With the basic principle of selectively melting metal powder. The energy source for the melting process is an electron beam emitted from a suitable cathode filament and is operated under high vacuum conditions. The electron beam is focused and scanned using a system of magnetic coils. EBM products are made from precursor powder of advanced metal alloys such as cobalt based alloys, nickel based alloys, titanium based alloys, copper alloy and stainless steel (316L) [7].

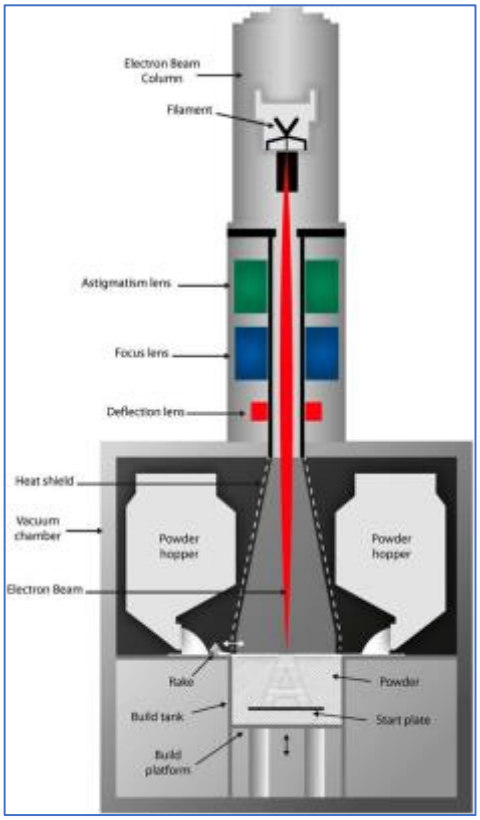

Figure 2 Schematic view of Arcam EBM system. Courtesy of Arcam EBM AB [8]

How it works?

The EBM system consists of powder hopper to locally store the metal powder to be used. The metal rake spreads the gravity fed powder from the hopper over the start plate or already existing powder layer. The nominal particle size distribution of powder used is 45-106μm and the melted layer thickness is ~50 to 100μm. The first powder layer is raked on a 'build substrate' or 'start plate' which functions as a mechanical support to the build material by preventing the movement of existing layers of the build when successive layers are raked out. It also acts as critical heat sink for heat dissipation from the build material during the printing process [3][9].

The next step is sintering of the powder bed layer by preheating to temperatures ranging from 600-1100°C. Sintering has mainly two important functions: a) to provide mechanical stability with the sintering of powder surrounding the plate, and b) to prevent 'smoking' which is the phenomena of particle ejection due to electrostatic repulsion of powder particles. This happens when along with energy, the interacting electrons also transfer electrical charge to the material producing repulsive electrostatic forces. Sintering the powder bed by diffused beam at rapid scan rates ($>10^4$ mm/s at high current) can help to increase forces holding the particles to the bed [3][9].

An electron beam with reduced scan rate and current ($>10^2$mm/s at <30mA current) is then used to selectively melt the powder bed. The cloud of electrons generated at the cathode is accelerated and focused by a system of magnetic lenses. This system provides very high scanning speeds (up to 1000m/s) without the need for moving mechanical parts. It also helps to achieve high build rates for EBM which is three to five times faster than other additive technologies [9][10].

Various scan strategies can be employed for selective melting. However, EBM commonly employs contour melting. According to this scan strategy, the beam first melts the boundaries of the part which acts as interface between the part and the surrounding metallic powder. The required part called as 'squares' is melted later by bi-directional scanning as shown in Fig. 3 [2][3].

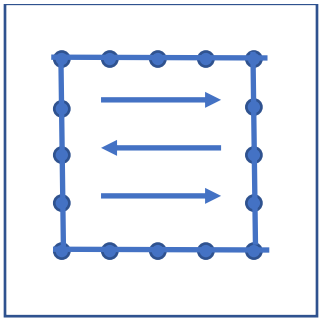

Figure 3 EBM scan strategy of contour melting.

As mentioned earlier, EBM parts are built under high vacuum condition. This is done primarily to increase energy efficiency by preventing the collision of fast moving electrons with air or gas molecules. The chamber pressure is maintained at $< 5 * 10^{-2}$ Pa. However, operating at high vacuum condition results in increased melt vaporization and 'smoking'. Therefore, build chamber pressure is raised to ~0.3 Pa during beam operation by injecting small quantity of helium gas which helps to reduce electrical charge build-up. Additionally, vacuum helps in additive manufacturing of reactive metals like titanium [3][10].

Important advantage with EBM system is the ability to temper residual stress by *in situ* heating of the material using the defocused electron beam. Residual stresses tend to build up in metallic AM materials because of the large thermal gradients during processing. This negatively affects the mechanical properties of the built part. In EBM system, sintering of the material bed results in higher operating temperature reducing the thermal gradient between peak melting temperature and powder bed temperature. The built part gets tempered *in situ* along with the building process. Previous work has shown that the residual stress in an EBM part is only 5-10% of ultimate tensile strength (UTS) [3].

Sintering of the powder bed however results in decreased recyclability of the excess powder. A powder recovery system is used to remove the excess powder from around the built part. Care has to be taken that chemical composition of the powder is within the specifications as recycled powder suffers from contamination from reaction with oxygen, nitrogen and other gases [3].

ASTM F75 Cobalt-Chromium Alloy

ASTM F75 is the standard specification for CCM alloy castings for surgical implants.

Table 1 Chemical composition of ASTM F75 [11]

Element	**Composition, % (Mass/Mass)**	
	Min.	**Max.**
Chromium (Cr)	27.00	30.00
Molybdenum (Mo)	5.00	7.00
Nickel (Ni)	-	0.50
Iron (Fe)	-	0.75
Carbon (C)	-	0.35

Silicon (Si)	-	1.00
Manganese (Mn)	-	1.00
Tungsten (W)	-	0.20
Phosphorus (P)	-	0.020
Sulphur (S)	-	0.010
Nitrogen (N)	-	0.25
Aluminium (Al)	-	0.10
Titanium (Ti)	-	0.10
Boron (B)	-	0.010
Cobalt (Co)	-	Balance

Table 2 As-cast mechanical requirements of ASTM F75 [11]

Property	
Ultimate tensile strength (UTS), min.	655 MPa
Yield strength (YS, 0.2% offset), min.	450 MPa
Elongation, min.	8%
Reduction of area, min.	8%
Hardness	25-35 HRC 266-345 HV

Other conventional standards for CCM alloys in the medical industry are:
ASTM F 799: Standard specification for CCM alloy forgings for surgical implants
ASTM F 1537: Standard specifications for CCM alloy wrought for surgical implants

Cobalt-Chromium Alloy applications

CCM alloys have found niche applications in nuclear, aerospace and medical industry. Some examples include being used to make valve seats for nuclear power plants and aerospace engine vanes and fuel nozzles. They are more widely used as biomedical surgical implants to make artificial hip and knee joints. It is reported that CCM alloy enables the use of metal on metal (MOM) bearings with large diameter femoral head components with minimum wear particles generated [11][12]. This also provides the advantage of increased range of motions than conventional artificial hip joints which mainly consisted of metal on plastic (MOP) or ceramic on ceramic (COC) joints. The latter two designs were prone to high wear particles being generated at artificial joints resulting in Osteolysis (disappearance of bone tissue) [12].

The above-mentioned applications rely on important material properties of CCM alloy such as strength at high temperature, corrosion resistance, excellent wear resistance and biocompatibility. The alloys are non-magnetic, have high mechanical strength and stiffness, and have mirror-like surface when polished.

Manufacturing techniques

Casting

Investment casting is the most common method used to manufacture surgical implants. The process is cheap and eliminates costly machining operations. However, strength and ductility of the cast CCM alloy is poor in comparison to what is required for implants. Dental castings were reported to occasionally fracture with small plastic deformation. The poor mechanical properties can be attributed to inherent casting defects such as large initial grain size, coring structure, solidification defects, and precipitation of alloys. These factors contribute to poor ductility and lower fatigue strength. The elongation to tensile failure values are reported to be

in the range ~1 to 12 % but mostly lies below 8 % which is required according to the ASTM F75 standard.

Hot forging
CCM alloys fabricated by hot forging process have better mechanical properties than cast because of the homogeneous structure and small grain size. These provides very good combination of tensile properties and elongation. However, the disadvantage with this technique is the difficulty to produce complex shapes like mesh structures.

Additive manufacturing by EBM
Both cast and wrought method need additional machining which increases the cost of production. Recently AM by EBM technology is emerging as a promising alternative method which can accurately create complex implants with minimum post machining [14][15]. It offers the advantage of creating complex solid geometries, reticulated mesh arrays, open cellular foams and complex, multifunctional components having varying densities and geometries for applications in biomedical, aeronautical and automotive industries [15].

One example is the manufacturing of total knee implants. It is composed of two parts: femoral and tibia knee stem. Efforts have been done to fabricate knee implants with varying density and porous structures. The porous surface will allow for efficient bone cell ingrowth and would eliminate the need for complex and failure prone surface coatings on implants manufactured traditionally [9].

Figure 4 EBM manufactured femoral knee components and tibia trays. Courtesy of Arcam EBM AB [16]

Literature study

Phases

According to the phase diagram (figure 5), CCM alloy consists of two primary phase matrixes: 1) γ-fcc phase 2) ε-hcp phase. The γ-fcc is the high temperature phase and is formed at room temperature by quenching the CCM alloy. The ε-hcp phase is the low temperature phase characterized by plate like striations (martensite) in the microstructure. The ε-hcp martensitic phase is known to enhance strength and wear resistance of the alloy but it also leads to low elongation or poor elongation. Various tensile test experiments on CCM alloys with ε-hcp phase as dominant phase have shown brittle fracture with poor elongation and UTS. It also results in high strain hardening exponent. One reason for its low elongation is the inherent low number of slip systems in hcp structures. It does not satisfy the Von Misses criteria in which five independent slip systems are required for good ductility. Carbide precipitation at grain boundary also results in poor ductility. On the contrary, γ-fcc metastable phase at room temperature has shown impressive elongation behaviour and UTS. Precipitation strengthening in the form of carbides and nitrides further improves the mechanical properties for room and high temperature applications [13] [17] [18][19][20]. Hence, considerable amount of research has been done to obtain metastable γ-fcc phase matrix for CCM alloys in comparison to ε-hcp phase matrix.

CCM alloy also consists of precipitates of the type [21]:

1) Carbides: $M_{23}C_6$:- {$(Cr, Fe, W, Mo)_{23}C_6$}
   M_6C :- {(Fe_3Mo_3C, Nb_3Co_3C)}
   M_7C_3 :_ {(Cr_7C_3)}
2) Nitrides: M_2N :- {Cr_2N}
3) σ-phase: Co-Cr intermetallic

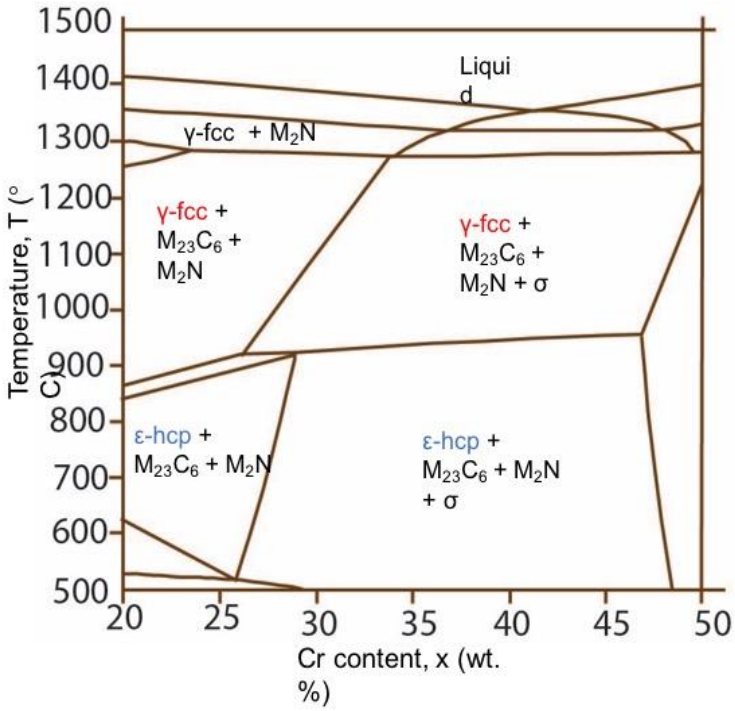

Figure 5 Phase diagram for Co-xCr-6Mo-0.23C-0.17N. Redrawn from [14]

ε-hcp to γ-fcc transformation

The hcp to fcc transformation (also called as martensitic transformation) can be induced in 3 ways:

1) Athermally (constant heat and temperature)
2) Isothermally (constant temperature)
3) Plastic straining

Stacking fault energy (SFE)

Before we proceed to elemental compositions of CCM alloy and effect of adding impurities, it is important to understand the relation between stacking fault energy (SFE) and ε-hcp phase formation.

Stacking faults (SF) are two dimensional errors in the stacking sequence and are characterized by a corresponding SFE. They are of two types: a) intrinsic stacking fault when formed by vacancy agglomeration, b) extrinsic stacking fault when formed by interstitial agglomeration. The reason behind dislocations splitting into partial dislocations is that dissociation leads to lowering of the total energy of the dislocation. A SF exists between two partial dislocations. Co and its alloys are found to possess low SFE [22]. According to thermodynamic calculations, SFE values become negative at temperatures lower than 827°C [13].

The stacking sequence for an fcc crystal is ABCABC or CBACBA and that for an hcp crystal is ABABAB, BCBCBC or CACACA. An example for SF in fcc structure is given in Fig. 6. Since {111} planes are the most densely packed planes in fcc metals, they are the planes upon which SFs exist [22]. SFs for γ-fcc phase can also be defined as plate of local ε-hcp phase in fcc matrix which has coherent interfaces with Shoji-Nishiyama (S-N) orientation relationship on each side facing the γ fcc matrix [14]. SFs are surrounded by Shockley partial dislocation for Co alloys.

Hence, it can be concluded that low SFE means high SFs and high Shockley partial dislocations formed. This results in high athermal ε martensite phase stabilized for CCM alloy because it is formed by regular overlapping of SFs. In other words, Shockley partials are precursors of ε martensite [13].

There are primarily three types of obstacles to Shockley partial dislocations [13]. Their effect on the strength and elongation of CCM alloy is given below.

1. Precipitates: presence of very fine carbides and nano-sized nitride precipitates are advantageous as they produce precipitation hardening and are responsible for very high strengthening effect in CCM alloy. They also produce the highest elongation with dislocations slipping over the precipitates.
2. ε-martensite plates: presence of ε martensite plates is unfavorable for the strength and elongation of CCM alloy. The interaction with Shockley partials results in strain induced martensitic transformation (SIMT) and premature fracture of the alloy.
3. Annealing twins: Like ε martensite plates, they interact with Shockley partials and act as preferential sites for formation of ε phase by SIMT. Also result in premature fracture.

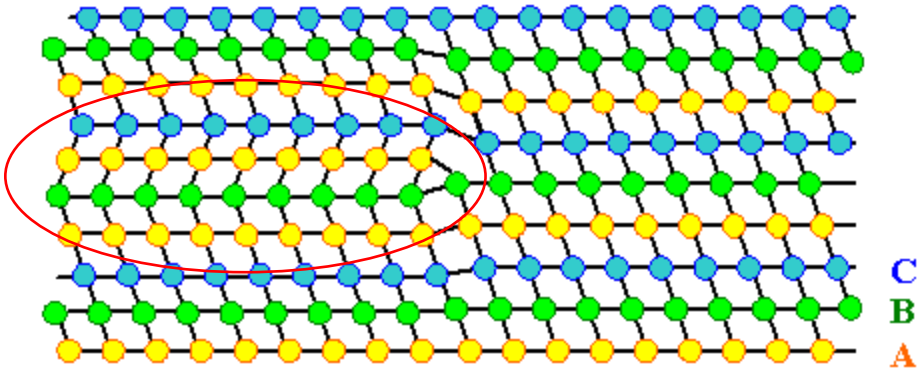

Figure 6 Representation of fcc crystal system

Co-Cr-Mo alloy compositions

Cobalt

Pure cobalt has two primary phases, low temperature ε -hcp phase and high temperature γ-fcc phase. The A_s transformation ε-hcp) to γ-fcc) takes place at ~460°C. While the reverse transformation (M_s) γ to ε takes place at ~390°C [15].

Chromium and Molybdenum

On alloying with chromium (Cr) and molybdenum (Mo), the ε to γ transformation temperature is significantly increased, i.e. it is 970 °C as shown in the figure 5 [15]. This substantial increase in transformation temperature happens because Cr and Mo reduce the Gibbs free energy (G) of the ε phase at temperatures lower than 1000°C [20]. Through carbide formation ($Cr_{23}C_6$, $Cr_{17}Co_4Mo_2C_6$, M_6C, M_7C_3), Cr improves the wear resistance, corrosion and oxidation resistance as well as hardness of the material. Molybdenum: also improves corrosion resistance of the alloy and by forming intermetallic Co_3Mo (hcp) phase, acts as a solid solution strengthener [15]. Both Cr and Mo are dissolved as substitutional elements in Co [19].

Two important trace elements are C and N whose compositions vary (according to ASTM F75, C<0.35 and N<0.25) and have significant effect on microstructure and corresponding mechanical properties.

Properties of CCM alloy without C & N

CCM alloys without C or nitrogen N have ε-hcp as the dominant phase and hence are prone to poor elongations and low tensile strength. Cast CCM alloys are found to have inter dendritic inclusions of σ phase at the grain boundaries [19]. σ-phase is tetragonal structure which consists of intermetallic compound of Co-Cr [21]. It gives rise to brittle fracture and poor UTS. Hence, it is favoured to remove σ-intermetallic phase from cast CCM alloy. One way to prevent preferential segregation of Co and Cr is by adding C and N. Interstitial N has high affinity for Cr and by interacting with Cr, makes it soluble in matrix and inhibits the formation of σ-phase [19]. Hence, as N increases, the σ-phase precipitate decreases. On the other hand, on adding C, carbides are formed according to the reaction $\sigma + C \rightarrow M_{23}C_6$ [23]. The fine carbides formed on intra-granular regions provide precipitation strengthening.

Ways to improve the strength of Co-based alloys:[23]

There are three primary mechanisms affecting the strength:

1) Solid solution strengthening (achieved by alloying Co with elements Cr, Mo, C and N)
2) Precipitation Strengthening
3) Grain refinement

Alloying with trace elements like C and N has been found to have significant impact on phase composition and corresponding mechanical strength of CCM alloys. In solid solution state, they occupy interstitial sites unlike Cr, Mo [19].

Nitrogen

As mentioned earlier, CCM alloys generally consist of two phases: metastable γ-fcc matrix and/or plate like ε-hcp martensite and this phase distribution significantly influences the mechanical and tribological properties. Thermodynamically stable ε phase and SFs enhance the strength and wear resistance of the alloy but drastically reduce the elongation of the alloy.

Early efforts were concentrated on optimizing the alloy composition, as well as casting and hot deformation properties. To prevent the wrought alloy to fracture due to presence of brittle ε martensite, nickel (Ni) was alloyed in large amounts (10-37 wt. %) conforming to biomedical CCM alloy standard ASTM F90 and F562. The alloy exhibited excellent ductility and found numerous applications [24][25]. However, Ni was later deemed inappropriate for biomedical implants as it causes allergies and cancer in living organism [4][5][13][17].

As a result, N was used to replace Ni to stabilize γ-fcc phase and increase the elongation of the CCM alloy that satisfy requirements of the type 5 criteria in ISO 22674 [17]. The maximum solid solubility of N in CCM alloy is ~0.35 wt.% (at 1200°C) [26]. The solubility is function of alloying content and C appears to decrease the solubility. N provides precipitates and stabilizes γ phase during cooling from melt by increasing the energy barrier for transformation from γ-fcc to ε-hcp via Cr-N cluster formation [7][27]. It also lowers the kinetic rate of γ to ε transition. The solubility of N increases up to 3 mass% on increasing the Cr content [20].

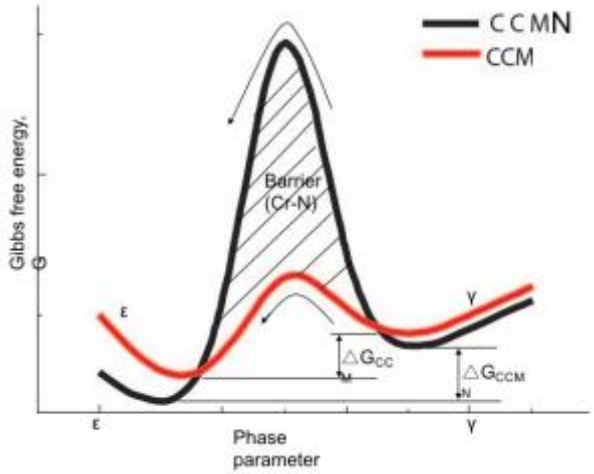

Figure 7 Schematic representation of γ phase stabilization by N addition. Redrawn from [27]

N atoms have strong affinity for Cr atoms and gathers around them to form N-Cr Interstitial-Substitutional (I-S) complex or N-Cr clusters. As a result additional forces are required for destroying or altering existing Cr-N clusters during γ to ε phase transformation [27]. The nitrides which are of nano metre size interact with the SFs and Shockley partial dislocations and inhibit their movement during phase transformation [13]. By this way, Cr-N clusters increases the energy barrier for γ to ε during solidification. Additionally, preferential interaction of Cr and N increases solubility of Cr in matrix and inhibits the formation of σ phase [19][20]. As seen in the phase diagram figure 5, σ phase consists of intermetallic compound Co-Cr and

when present as precipitate, decreases the elongation of CCM alloy. Co and Cr are found to segregate preferentially in σ phase precipitate in absence of C and N [23].

N also increases the SFE of the alloy[19]. With the increasing SFE, γ-fcc phase is more stable than ε-hcp phase and less crystal defects like dislocations and stacking faults are observed. Kenta et all has shown that with increasing N content to 0.24% by weight, there is a transition from highly planar dislocation arrays and wide SFs for no nitrogen CCM alloy to non-planar dislocations with narrow SFs [13]. Quenched ingots with N content greater than and equal to 0.10 wt. % after homogenization in γ phase region (1474 K, 30 mins) had γ phase stabilized at room temperature and no ε phase striations were found. They showed the highest elongation of 25%. The elongation decreases with further increasing the N content. This is because the percentage of annealing twins increases with N content and act as obstacles to Shockley partials leading to SIMT and site for crack nucleation.

Table 3 Mechanical properties of hot forged and quenched CCM-N alloy with different nitrogen concentration. Adopted from [13]

	0N	**0.05N**	**0.07N**	**0.10N**	**0.17N**	**0.24N**
Phase	γ+ε	γ+ε	γ+ε	γ	γ	γ
YS	-	-	-	-	507MPa	587MPa
UTS		728Mpa			931	962
Elongation%	11.5	9.9	17.1	24.1	22.5	20.4
Annealing twins	0	0	5%	60%	70%	75%
Fracture surface	Facet	facet	facet	facet	facet	facet

The above table provides mechanical property of hot forged and quenched CCM-N alloy. The ideal N concentration for better mechanical strength and elongation is in the range 0.10<N<0.24 wt. %.

Carbon

C is another important trace element studied in this thesis. In the dissolved state, it provides solid solution strengthening to CCM alloy. With C addition, precipitates in the form of carbides are formed. Presence of fine carbides in the intra-granular region increases the alloy strength and ductility (i.e. precipitation strengthening). However, they are detrimental to fatigue strength of the alloy when present at the grain boundaries. Carbides are also responsible for producing grain refinement during solidification. According to Hall-Petch relationship, the finer grain size results in increased YS and UTS.

Like N, C also plays and important role in stabilizing γ-fcc phase of CCM alloy during solidification. It does this by decreasing the Gibbs free energy of the γ fcc phase relative to ε hcp phase [7]. Sang et all showed that for quenched equi-axed CCM-C alloy samples, with increasing carbon concentration from 0 wt. % to 0.18 wt. %, the volume fraction of γ phase increased from 12 % to 30 % [28]. This resulted in increase in UTS and highest elongation of 30% at 0.1 wt. % of carbon. Carbon also increases the SFE and decreases the density of SFs of the alloy which in turn stabilizes the γ-fcc phase. One thing to note is that elongation decreases with carbide precipitation. No carbides precipitate for 0.1 wt. % C but fine carbides precipitate for 0.18 wt. % C. Even though UTS increases, since carbides act as preferential sites for crack nucleation and propagation, elongation decreases for CCM-C alloy when carbides precipitate.

With the ideal concentration of N discussed above, it's time to consider the effect of changing C concentration on CCM-CN alloy fabricated by hot forging process where the N concentration is fixed at 0.20 wt. % [23]. There is considerable increase in 0.2% YS from 0.05 to 0.19 wt. % C. There is not much change in UTS with highest for 0.10 wt. % C. However, there is a drastic drop in elongation percentage to below 10% for 0.24 wt. % C. Important thing to consider here is the presence of γ-fcc dominant phase in the matrix for all C concentration. As discussed earlier, for CCM-N alloy with 0.20 wt. % N, γ-fcc was the dominant phase matrix. Hence, the effect of phase matrix on the changing mechanical property with varying carbon concentration can be neglected.

Very fine carbide precipitates are found at intra-granular regions for C concentration ≥ 0.10 wt. % and are responsible for the increase in YS. However, the increase in C concentration is believed to have increased the volume fraction of fine carbides. Few coarse carbides of submicron size (< 1μm) were also observed for higher C concentration alloy. Since there is very low volume fraction of initial ε-hcp phase, excessive C concentration and carbide precipitation can lead to decrease in ductility of the alloy.

Table 4 Mechanical properties of hot forged and quenched CCM-CN alloy with 0.20 wt. % N and varying C concentration. Adopted from [23]

	0.05C	**0.10C**	**0.15C**	**0.19C**	**0.24C**
Phase	γ	γ	γ	γ	γ
YS	775MPa	800MPa	900MPa	950MPa	995MPa
UTS	1300MPa	1400Mpa	1350MPa	1330MPa	1300MPa
Elongation%	37	33	18	12	10
Annealing twins	Almost the same				
Fracture surface	facet	facet	facet	dimple	dimple

The above table provides mechanical property of hot forged and quenched CCM-CN alloy. The ideal C concentration for better mechanical strength and elongation is in the range 0.05<C<0.10 wt. %.

Deformation modes

The deformation modes observed in CCM alloy are:

1. Deformation twinning
   Modes of formation of twins [22]:
   1. Growth twins: result of change in lattice during crystal growth due to possible deformation from a larger substituting ion.
   2. Annealing or transformation twins: result of change in crystal system during cooling as one form becomes unstable and the crystal structure must re-organize or transform into another more stable form.
   3. Deformation or gliding twins: are result of stress on the crystal after the crystal has formed. They in general correspond to rotation, or axial, twins.

   For any polycrystalline, five independent shear systems are required for deformation to occur. Twinning is an important deformation mechanism for crystals with a limited number of slip systems where they operate to provide the five systems. Thus, deformation twinning is pronounced in hcp crystals since hcp phase is characterised by limited dislocation slip system. Twinning is also observed in high symmetry crystals

like fcc during deformation at low temperatures. They also act as obstacles to the motion of slip dislocations, providing sites for pileups and consequently for fracture nucleation.

Deformation twins is the dominant deformation mode observed for pure Co hcp phase structure where the tension twins of {1012} constituted ~82.1% of the twins. This is because of the very low SFE of pure Co as compared to SFE of CCM alloy [29].

2. Shockley partial dislocation motion leading to Strain Induced Martensitic Transformation
   For CCM alloys with γ fcc phase matrix, the dominant deformation mode is Shockley partial dislocation motion bounding the SF on {111} plane [30]. As mentioned earlier for fcc crystal system, the {111} planes are the planes upon which SFs are formed. According to the overlapping model during deformation, various SFs accumulate and overlap to form ε hcp phase [31]. This is called SIMT in γ phase matrix. SIMT is generally nucleated at two sites: 1) annealing twin boundaries 2) grain boundaries/random boundaries.

   Lee et al has presented that during tensile testing of CCM-0.04C-0.16N, cracks have nucleated at triple junction i.e. two random boundaries and one annealing twin boundary. The triple junctions are the sites of maximum atomic misfits. As strain increases, the thickness of ε hcp phase increases. The cracks have propagated along the annealing twin boundaries or along the interface between the ε-hcp and γ-fcc phase. The fracture morphology consisted of {111}-fcc or {0001}-hcp stepwise cleavage surface [31]. This happens because of the semi-coherent interface between strain induced ε-hcp and γ-fcc phase and by accumulation of stresses. Since ε hcp phase is characterised by limited dislocation slip systems, high rate of work hardening is observed during plastic deformation. Moreover, annealing twins plays an important role for the cleavage-type fracture for low SFE CCM alloy as it acts as sites for nucleation of SIMT as well as for crack initiation and propagation during deformation of the alloy.

3. Slip system
   For fcc CCM alloy crystal system, the {111} planes are the most densely packed planes and are also the planes upon which SFs are formed. They are also the glide planes and coherent twin planes and deformation of the alloy is accompanied by twinning on this plane to the dislocation slip [22].

   For hcp CCM alloy crystal system, extended dislocations on (0001) basal plane have been observed. The low SFE of CCM alloy favours this as the slip plane. However, it also correlates with the c/a ratio. of slip systems of hcp phase [22].

   Simultaneous activation of basal <a> slip and prismatic <a> slip: According to EBSD analysis and TEM observations, it was revealed that for strain <10%, dislocation slip lying on (0001) basal plane and {1100} prismatic plane is the dominant deformation mode in CCM alloy with ε hcp phase matrix[30][29]. Initial observations have shown striations for strained CCM alloy (ε hcp phase), corresponding to either slip planes or twinning. However, no disorientations were found among these striations, leading to conclusion that it occurs by slip lines. The change in dominant deformation mode from deformation twins in pure Co (with ε phase matrix) to simultaneous activation of basal <a> slip and prismatic <a> slip for CCM alloy (with ε phase matrix) is speculated to be because of relative increase in SFE values of the CCM alloy[29].

Additionally, slipping is also believed to be the dominant deformation mode for γ-phase matrix CCM-CN alloys with precipitates. Shi et al had presented that no ε-hcp phase was observed by EBSD analysis on the fracture surface of the tensile specimen which had single γ-phase matrix before the test and had elongations of 12.6% [14]. The same was confirmed by Manami et al with the fracture morphology of dimple type [23]. The reason for this behaviour where SIMT is retarded is speculated to be because of the presence of precipitates in the form of carbides and nitrides as the ε-phase peak on XRD graphs of fractured surface decreased with increasing concentration of C and N. The precipitates on the {111} plane of γ-fcc phase impedes shear deformation on the {111} slip plane and obstructs the movement of Shockley partial dislocations and thereby prevents SIMT.

Table 5 Deformation modes & fracture surface morphology of CCM alloys

Alloy	**Dominant Phase**	**Dominant Deformation**	**Fracture Surface Morphology**	**Reference**
Pure Co	ε-hcp	Deformation twinning	Facet-type	[29]
CCM	ε-hcp	Basal <a> slip and Prismatic <a> slip	Facet-type	[29][30]
CCM-0.16N	γ-fcc	SIMT	Facet-type	[30][13]
CCM-0.05C	γ-fcc	SIMT	Facet-type	[32]
CCM-0.05C-0.16N	γ-fcc	SIMT	Facet-type	[23][31]
CCM-0.24C-0.16N	γ-fcc	Twinning or Slipping	Dimple	[23]
CCM-0.23C-0.17N EBM built	γ-fcc	Twinning or Slipping	Dimple	[14]
CCM-0.23C-0.17N EBM built after ageing at 800°C for 24hrs	ε-hcp	Basal <a> slip and Prismatic <a> slip without cross-slipping from basal to prismatic	Dimple	[14]

Hot isostatic pressing (HIP)

HIP can be defined as a thermomechanical process for material fabrication in which metal powder or a pre-moulded shape is simultaneously subjected to both high temperature and high isostatic pressures using a gas transfer medium. The term ‘isostatic pressure’ means that the pressure is applied on the material from all directions. The main aim is to achieve high density in the treated material with refined-pore free microstructure and grain size. This is achieved through a combination of plastic deformation, creep and diffusion bonding. Since its first use in 1960 for fabricating nuclear fuel clad, the process has found broad range of industrial applications. These include: post densification of sintered cemented carbides or metal parts (specialty steels), healing of fatigue or creep induced damage in superalloys and titanium castings, and heat treatment and porosity elimination of cast parts.

Argon is the most commonly used gas to transmit pressure because of its inert nature. Pressure used is in the range 70-300 MPa. Since the material is subjected to pressure along with temperature in HIP, it provides an added advantage over isothermal sintering procedures in which densification is achieved at approximately 25-50% higher temperature than what is used in HIP. As shown in the table 6, HIP systems are composed of four basic units: pressure vessel, internal heater (furnace), pressurization and control unit [33][34][35][36].

CCM alloy parts fabricated by EBM technique are heat treated for HIP to remove the manufacturing defects and to also increase the elongation property. Kircher et. all have found that as-built EBM manufactured CCM-0.22C-0.14N material is very brittle and easily fractures when stressed parallel to the build direction [37]. After HIPing and homogenization, there is drastic change in mechanical properties observed. The YS decreases but elongation increases considerably.

The recommended HIP cycle for CCM-CN alloy is as follows:

Table 6 HIP Treatment parameters [16]

Time	**Temperature (K)**	**Pressure (Mpa)**	**Atmosphere**	**Cooling**
4 hours	1473	100	Argon	Free cooling rate

Experimental techniques

Sample preparation

Small cubical samples with 3 different C and N content were printed in EBM machines (new Q series) with similar processing parameters. One batch of samples were then HIP treated. The HIP treatment was similar to recommended treatment in table 6. All the samples for this thesis were within the range of ASTM F75 standard and were provided by Arcam EBM AB. For microstructural characterization, the 6 samples (3 in as-built condition, 3 in HIP condition) were then cut in two cross sections: vertically (parallel to build direction) and horizontally (perpendicular to build direction). The microstructures were characterized by optical microscopy (OM), scanning electron microscopy (SEM) with electron back scattered diffraction (EBSD) and X-ray diffraction (XRD). For mechanical strength, Vickers micro-hardness test was done on horizontal cross sections. From here on the samples will be denoted by their C content only. The corresponding N content will be implied automatically.

Table 7 Chemical composition of the samples

		As-built	
		Horizontal cross section	Vertical cross section
HIP	Horizontal cross section	0.05 wt.% C – 0.056 wt.% N 0.10 wt.% C – 0.093 wt.% N 0.15 wt.% C – 0.13 wt.% N	
	Vertical cross section		

The cut cross sections of the samples were embedded in Polyfast-hot mounting polymer resin which is electrically conductive. They were then grinded and polished using 9πm, 3πm and 1πm abrasive size respectively. The last step included polishing with oxide polishing suspensions (OPS) until no scratches were visible. Finding the right etchant involved using trial and error method in which several etchants were tried starting from weak acids to strong acidic mixtures until a satisfactory microstructure was observed. It was observed that CCM alloy has high corrosion resistance with completely different reactivity to chemicals for as-built and HIP samples. Best results were obtained by electrolytic etching for 15-30 seconds in 30 % HCl solution with few drops of H_2O_2 at 4V, graphite electrode. Care must be taken that sample surface is freshly polished using OPS solution. The table below lists the etchants tried [21][38][39]:

Table 8 Etchants list

Number	**Etchant**	**Remarks**
1)	6HCl: $1H_2O_2$	No reaction
2)	12HCl: $1H_2O_2$	As-built samples etched, only carbides observed, no grain boundaries No reaction with HIP samples
3)	100ml H_20 + 50ml HCl + 10ml HNO_3 + 10g $FeCl_3$	No reaction
4)	20HCl: $1H_2O_2$	No reaction
5)	Waterless Kalling's reagent 5g $CuCl_2$ + 100ml HCl + 100ml Ethly alcohol	As-built samples etched on agitation, only carbides observed, no grain boundaries No reaction with HIP samples
6)	Kalling's reagent	As-built samples etched on agitation, only carbides observed, no grain boundaries

	6ml H_2O + 6g $CuCl_2$ + 60ml HCl	No reaction with HIP samples
7)	Glyceregia	No reaction
8)	Acetic glyceregia	No reaction
9)	Electrolytic etching 10% HCl solution, 4V, graphite cathode	As-built samples etched No reaction with HIP samples
10)	Electrolytic etching 30% HCl + few drops of H_2O_2, 4V, graphite cathode	As-built and HIP samples etched

Microscopy

OM was performed using Leitz DMRX microscope. It works by illuminating flat, polished and etched samples by light. Based on physical and chemical differences like phase composition, surface morphology, the beam is reflected in different ways. Different magnification lenses are used to produce desired image with maximum resolution of ~1µm. SEM was performed using LEO Gemini 1550 (Field Emission Gun –SEM) and Philips XL 30 (Environment-SEM). In SEM, resolution as high as ~10nm. In this technique, the sample is scanned using focused electron beam under vacuum condition. The electrons interact with the atoms of the sample at or near the surface and by choosing different detectors, various signals of measurement are obtained e.g. backscattered electrons, secondary electrons.

Electron back scattered diffraction

EBSD technique provides microstructural and crystallographic information e.g. local texture, grain morphology, grain boundary distribution, grain size and grain size distribution [40]. The system comprises of a Nordlys II EBSD detector coupled with a Channel 5 software by HKL technologies. It measures and identifies electron backscattered diffraction pattern (Kikuchi patterns) which are characteristic of the sample crystal structure and the position from where it was measured. To obtain this pattern, the sample is tilted 70° towards the EBSD detector (figure 8) and the incident electron beam is scattered elastically at the atomic planes of the sample. The diffracted electrons are then captured on phosphor screen. The software indexes the obtained pattern by comparing it with crystallographic data of the expected preselected phase. Complete colour spectrum is used to address the measured orientation. However, when a pixel hits undefined phase (e.g. grain boundary, impurities, sample preparation and etching defects) or due to poor pattern quality, indexing is undefined and the software gives "zero solution" or in other words "no solution" for that pixel. To perform phase analysis on the samples, a pre-defined area was scanned using a step size of 0.5µm and working distance in the range of 14-18 mm.

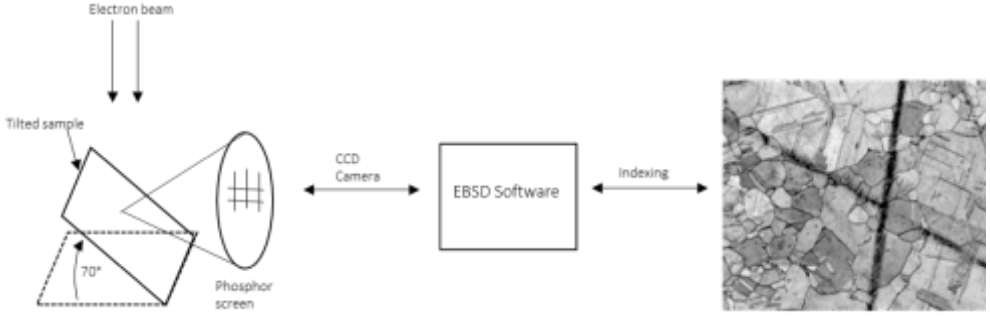

Figure 8 Representation of EBSD system

X-ray diffraction

XRD technique measures the inter-planar spacing of crystalline materials and provides information about phase composition, atomic structure, residual stresses etc. Monochromatic X-ray beam is incident on the sample at various Θ (diffracted angle) angles and the corresponding diffracted beam intensity is measured by the rotating XRD detector as a function of 2Θ angle. The incident beam is diffracted at the lattice of the crystal and follows the Bragg's law. The measured intensity is then plotted to give XRD pattern. The pattern is then compared with that of a powder standard (has a random texture) found in the database. XRD analysis was performed using Bruker D8 X-ray diffractometer having Chromium anode (wavelength 2.28970 Å). The measurement parameters were a) Θ range 30° to 145° b) step size = 0.08 c) rotation speed = 15 rpm d) generator power 35 kW and 40 mA. XRD was carried on horizontal cross sections and had polished surface to reduce background noise and were naked (i.e. not embedded in polymer mount).

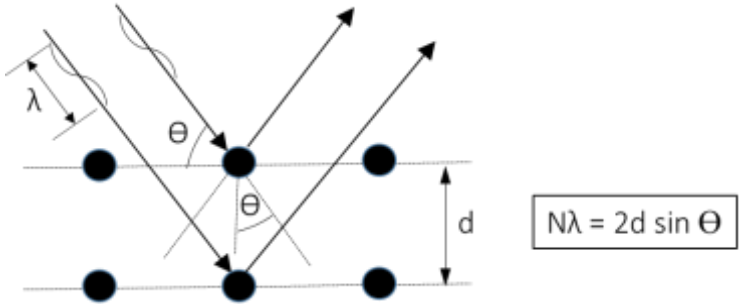

Figure 9 Representation of Bragg's law of diffraction

The XRD peaks for the samples were identified by matching with two CCM alloy Phase Diffraction File (PDF) standards which are developed by ICDD (The International Centre for Diffraction Data). They are PDF 04-016-6869 for γ-fcc phase and PDF 04-016-6870 for ε-hcp phase. Various factors characterize the absolute and relative intensities of the lines in a XRD material pattern. They are structure sensitive, instrument sensitive, sample sensitive and measurement sensitive. Only one among these factors is concentration of analyte (i.e. the species being measured). Reference Intensity Ratio (RIR) was used for semi-quantification of phases present. It is assumed that all other factors except concentration of analyte are rationed and reduced to a constant. This method is based on scaling all diffraction data to the diffraction data of standard reference materials (corundum). It is based on the formula

$$\frac{I}{I_c} = \frac{\mu\gamma\rho_c}{\mu_c\gamma_c\rho} \text{ [41]}$$

where μ = linear attenuation coefficient, γ = absolute scale factor, ρ = density and subscript 'c' corresponds to corundum.

Micro-hardness

Micro Vickers hardness test was performed using Wolpert Probat machine. 10 indents were made on horizontal cross sections of each sample with a load of 10kg. After measuring the average diagonal to the indent, Vickers micro-hardness value were calculated according to the formula [42]:

$$\frac{Test\ force\ (kgf)}{Surface\ area} = HV$$

Observations

Microscopy

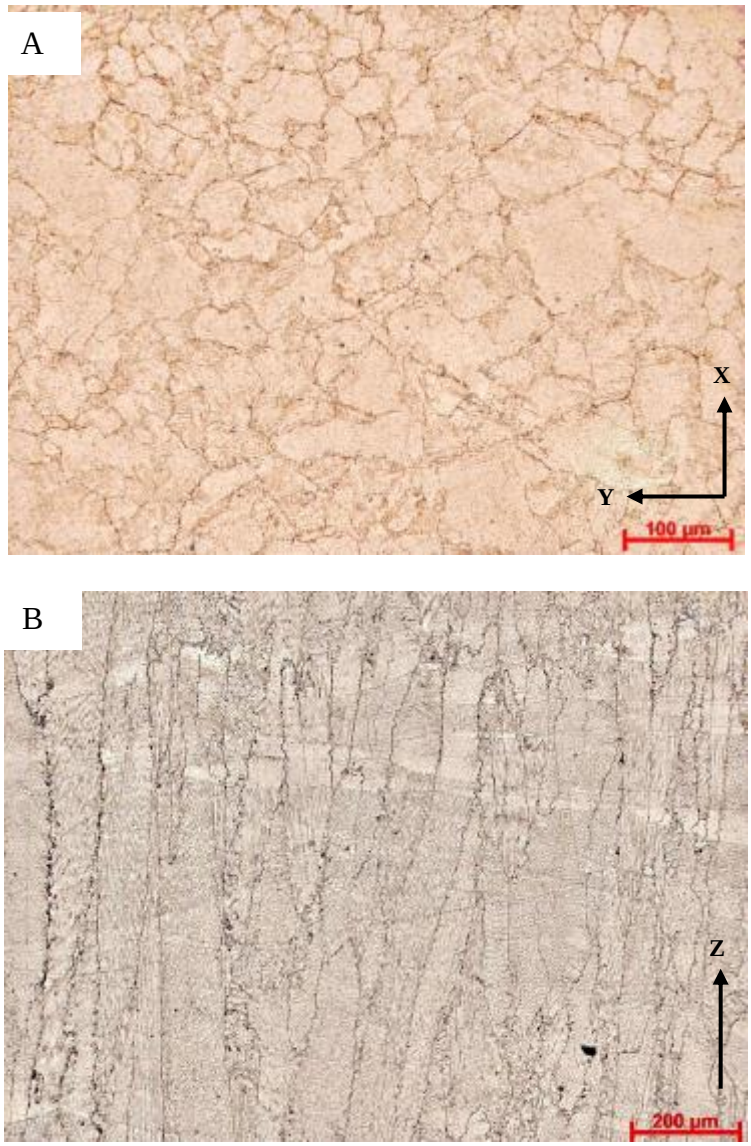

Figure 10 OM images for 0.05 wt. % C as-built condition in cross-sections A) horizontal B) vertical

Figure 10 illustrates the OM images for as-built 0.05 wt. % C. In the vertical cross sectional view, long columnar grains have grown parallel to the build direction. This is a typical microstructure for EBM processes. The width of the grains averages in the range ~50 to 70µm. The precipitates are distributed regularly in zig-zag pattern inside the grains. This pattern may be arising because of systematic shift in the beam scan either for preheating or successive layer melting. In the horizontal cross sectional view which is the top view of the columnar grains, the grains are of equi-axed dimensions with carbide rich precipitates distributed inside the grains. The grain boundaries are difficult to distinguish from precipitates at the grain boundaries. However, the precipitates seem to be uniformly distributed. They may be formed during electron beam scanning for preheating and successive melting.

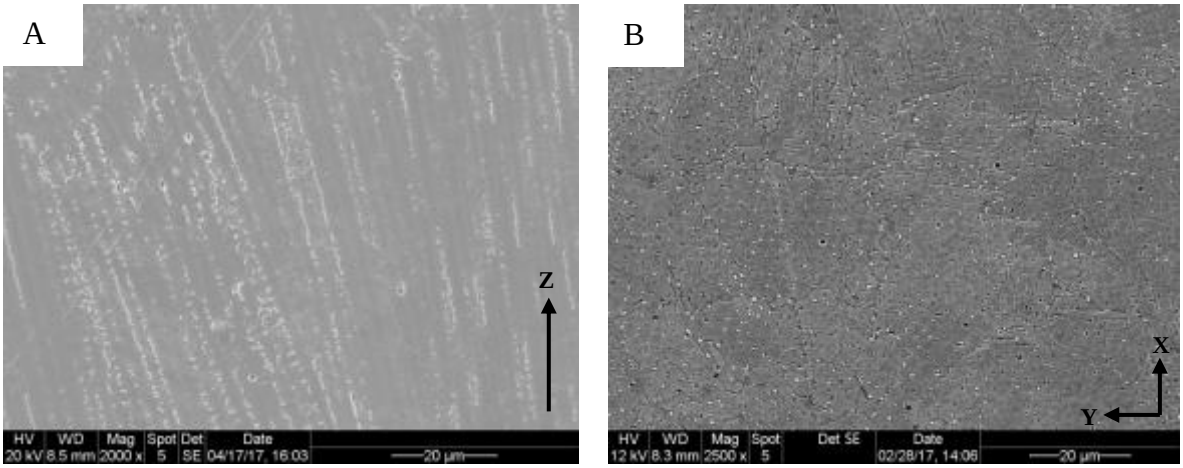

Figure 11 SEM images for 0.05 wt. % C as-built condition in cross-sections A) vertical B) horizontal

Figure 11 shows the magnified images of as-built microstructure. Cylindrical precipitates elongated along the build direction can be seen in the vertical cross sectional view. They are homogeneously distributed and appear as globular precipitates of size ~2µm in the horizontal cross sectional view.

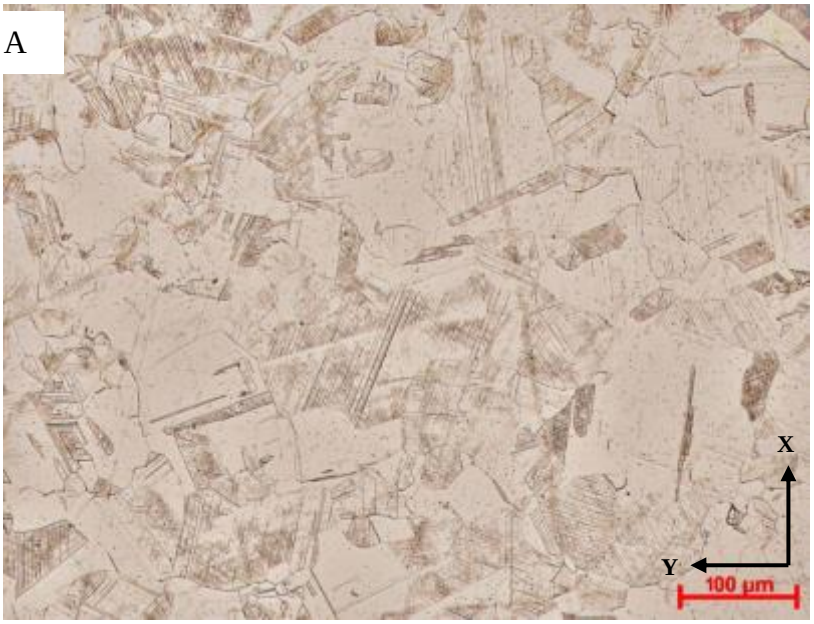

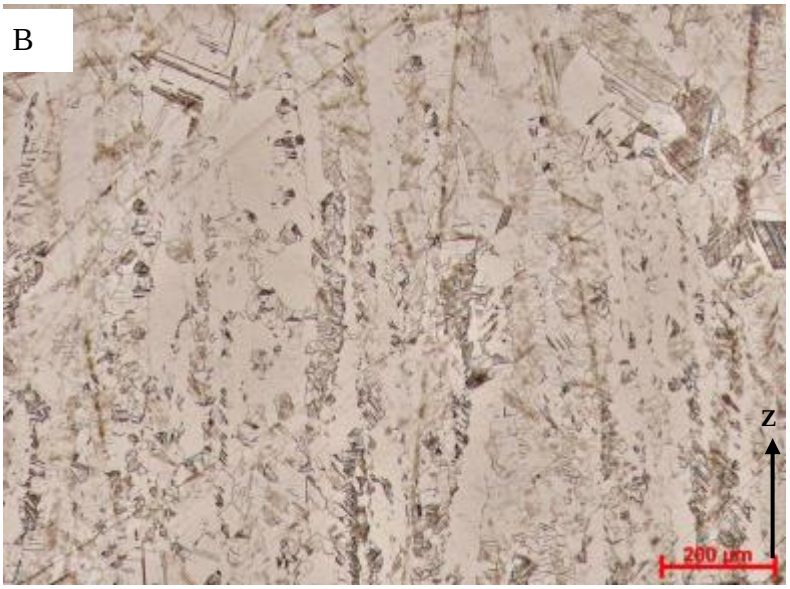

Figure 12 OM images for 0.05 wt. % C HIPed condition in cross-sections A) horizontal B) vertical

Figure 12 illustrates the OM images for 0.05 wt. % C after the HIP treatment. There are two main observations. First is partial dissolution of the precipitates. Second is recrystallization of grains. In the horizontal cross sectional view, large fraction of precipitates has dissolved in the matrix and there is negligible change in the grain size. Significant fraction of striations are observed that run throughout or partially inside the grains. The striations are of straight shape and distributed in 'grid' pattern with two parallel sets crossing each other. In the vertical cross sectional view, inhomogeneous grains are observed. At certain areas, new smaller grains have formed inside long columnar grains. At other areas, the columnar grains are still preserved. Like in the HIPed horizontal cross section microstructure, partial dissolution of the precipitates has occurred. Striations are randomly distributed inside the grains.

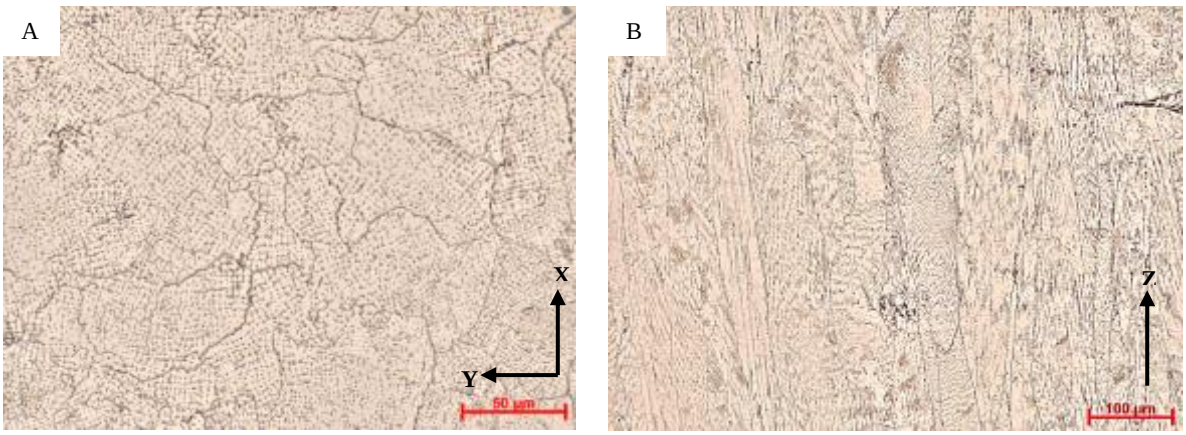

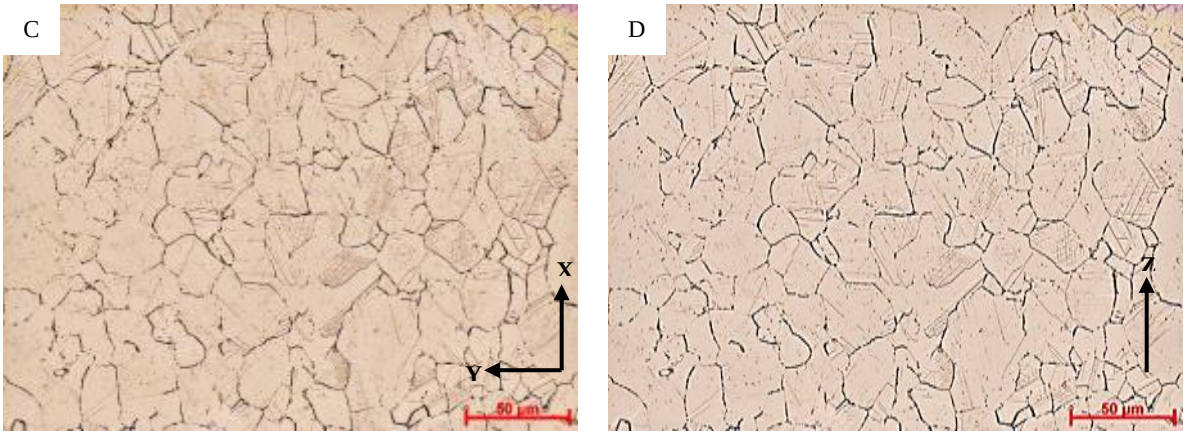

Figure 13 OM images for 0.10 wt. % C, A) & B) in as-built condition for horizontal and vertical cross-section respectively, C) & D) in HIPed condition for horizontal and vertical cross section respectively.

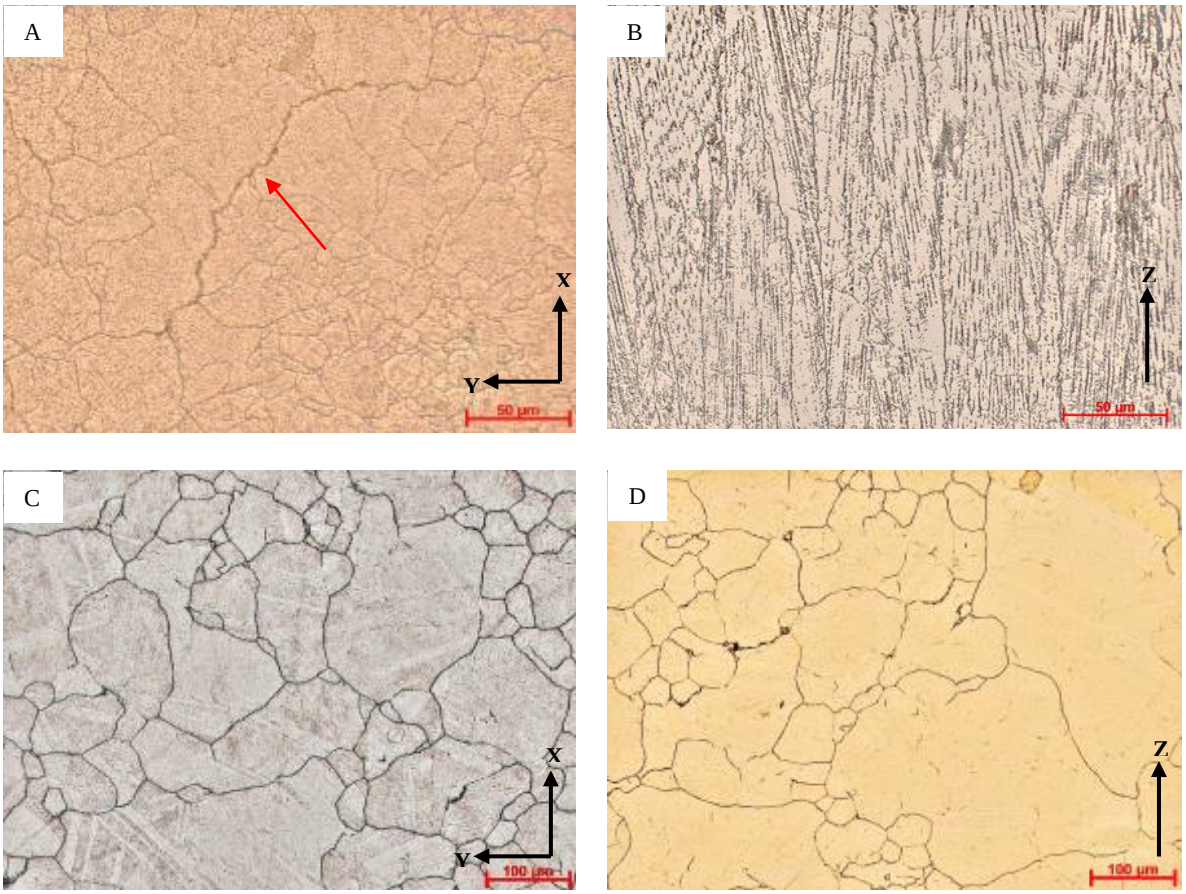

Figure 14 OM images for 0.15 wt. % C, A) & B) in as-built condition for horizontal and vertical cross-section respectively, C) & D) in HIPed condition for horizontal and vertical cross section respectively.

The as-built microstructure is similar for all carbon content except for some cracks (red arrow in figure 14-A observed in 0.15 wt.% C. However, unlike in 0.05 wt.% C after HIP, all the columnar grains in vertical cross section have transformed to equi-axed grains for 0.10 and 0.15 wt.% C. Grain growth is also observed for 0.15 wt.% C HIP condition.

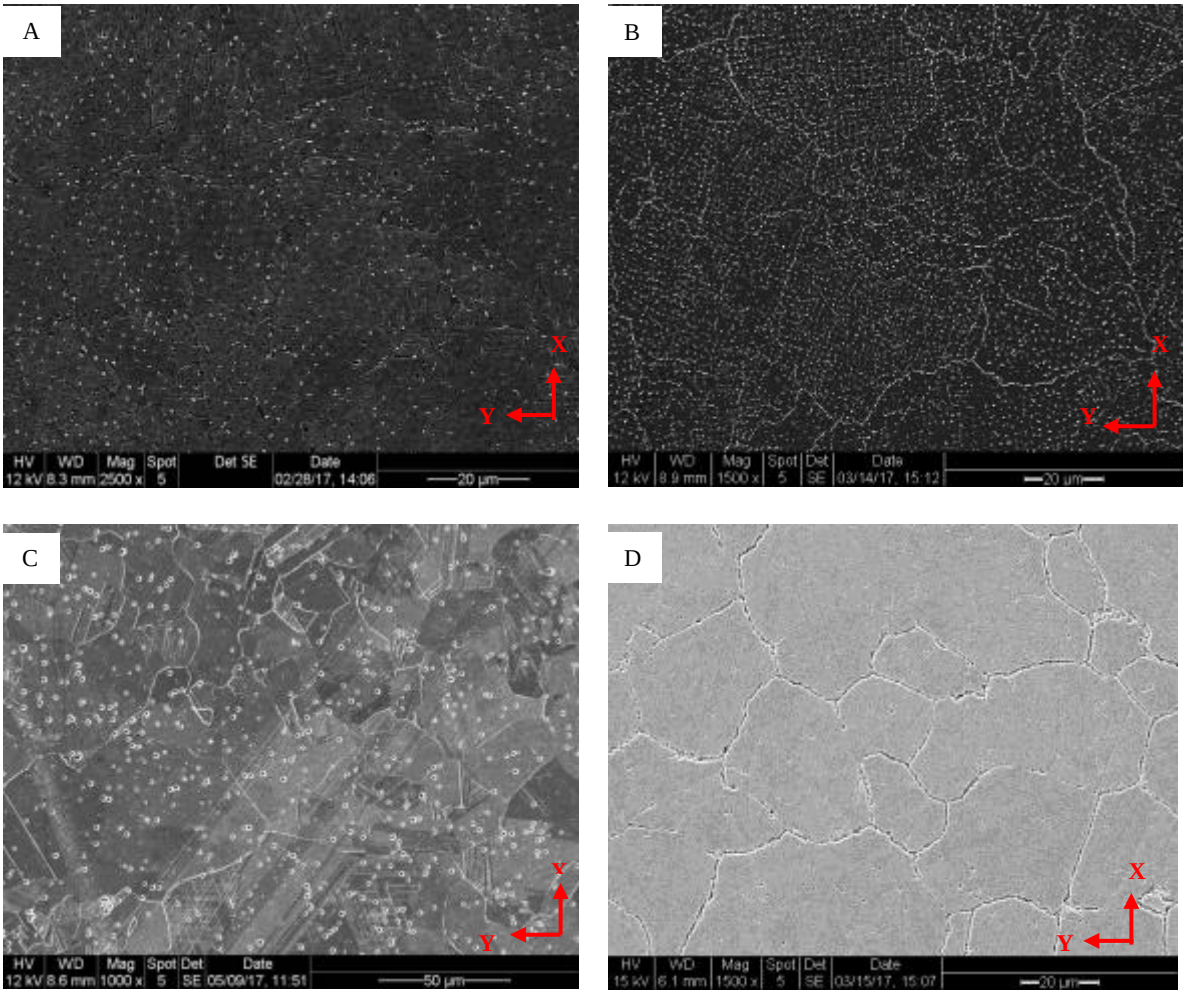

Figure 15 SEM images showing precipitation distribution for A) & B) as-built condition 0.05 & 0.15 wt. % C respectively, C) & D) HIP condition 0.05 & 0.15 wt. % C respectively

On taking closer look at the microstructure in SEM (figure 15), an increase in percentage of precipitation is visible with increasing carbon content for as-built condition. For 0.15 wt.% C, the grain boundaries are decorated with precipitates along with in-grain precipitation. Only in-grain precipitation can be seen for 0.05 wt. % C. After HIPing, globular cavities can be seen for 0.05 wt.% C and continuous cavities at the grain boundaries can be seen for higher carbon content samples. The cavities may have formed in place where the precipitates got etched away during electrolytic etching.

Observations

Phase analysis

XRD results:

Graphs

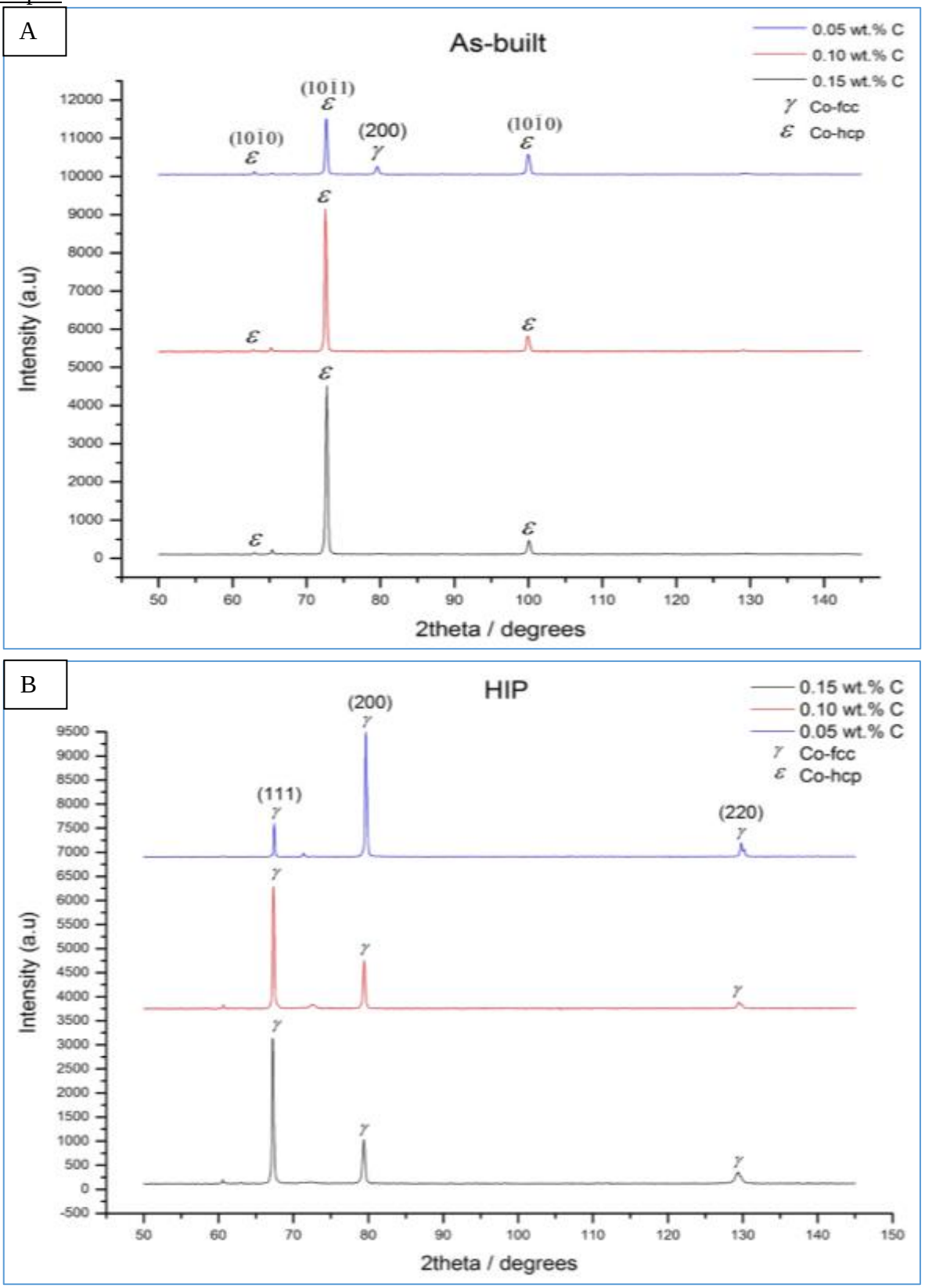

Figure 16 XRD pattern for A) as-built samples with different carbon concentration, B) HIP samples with different carbon concentration

Observations

The volume percentage of different phases is as follows:

As-built	**γ-fcc Vol %**	**ε-hcp Vol %**
0.05 wt.% C	11%	88.70%
0.10 wt.% C	0.50%	99.50%
0.15 wt.% C	0.50%	99.50%

HIP	**γ-fcc Vol %**	**ε-hcp Vol %**
0.05 wt.% C	99.5%	0.50%
0.10 wt.% C	99.5%	0.50%
0.15 wt.% C	99.5%	0.50%

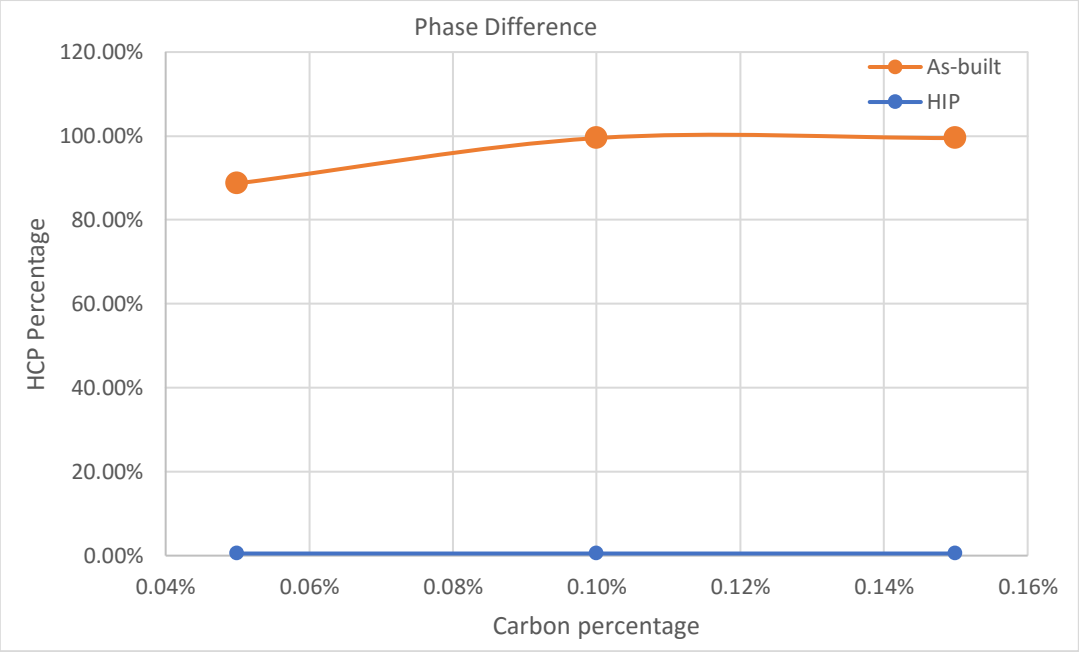

Figure 17 HCP phase difference in as-built and HIP samples

As calculated from the XRD peaks, samples in the as built condition have ε-hcp dominant phase. During the EBM process, melting and solidification of the powdered layer is very fast (within seconds). This means that the high temperature metastable γ-fcc phase should be found in the solidified CCM-CN alloy. S. H. Sun et al observed columnar grains with γ-fcc dominant phase in the longitudinal cross section of the top part of EBM as built sample (total height 85mm) [7]. However, ε-hcp phase is dominant in the investigated as built samples. This may be because of high build temperature which is a characteristic of EBM additive manufacturing process. Diffused beam is used to sinter the powder bed which rises the build temperature to approximately 600-800 °C. The whole build is held at this elevated temperature during the complete build time of approximately 25-30 hours. This extended post built heat treatment induces phase transformation from metastable γ-fcc phase to stable ε-hcp phase. Since the samples for microstructural analysis where printed in small cubes and taken close from the build plate, they are expected to have undergone isothermal martensitic transformation. According to temperature-time-transformation (TTT) diagram for CCM-0.23C-0.17N alloy, isothermal phase transformation initiates after 48 hours at 650 °C and after 7 hours at 700 °C (figure 18)

[7]. The percentage of phase transformed ε-hcp is less in 0.05 wt. % C than for 0.10 and 0.15 wt. % C as built samples.

For the HIPed samples, γ-fcc is the dominant phase for all carbon concentration. This indicates that during hot isostatic pressing at 1473 K major phase transformation from ε-hcp to γ-fcc took place. With subsequent free cooling, metastable γ-fcc phase has been preserved at room temperature. The γ-fcc phase with equi-axed grains in the HIPed samples may lead to better UTS and elongation properties.

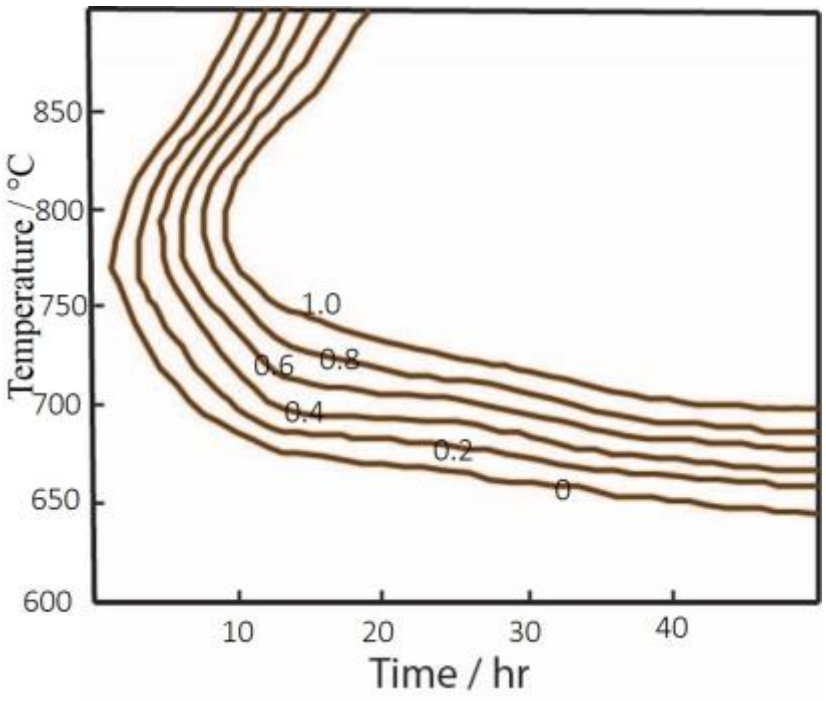

Figure 18 TTT diagram of γ phase transformation during isothermal heat treatment. Redrawn from [7]

Observations

EBSD results

Scan 1

The EBSD phase analysis was done for as-built vertical cross sectional 0.05 wt. % C sample. The whole image in fig. 19-A) was scanned:

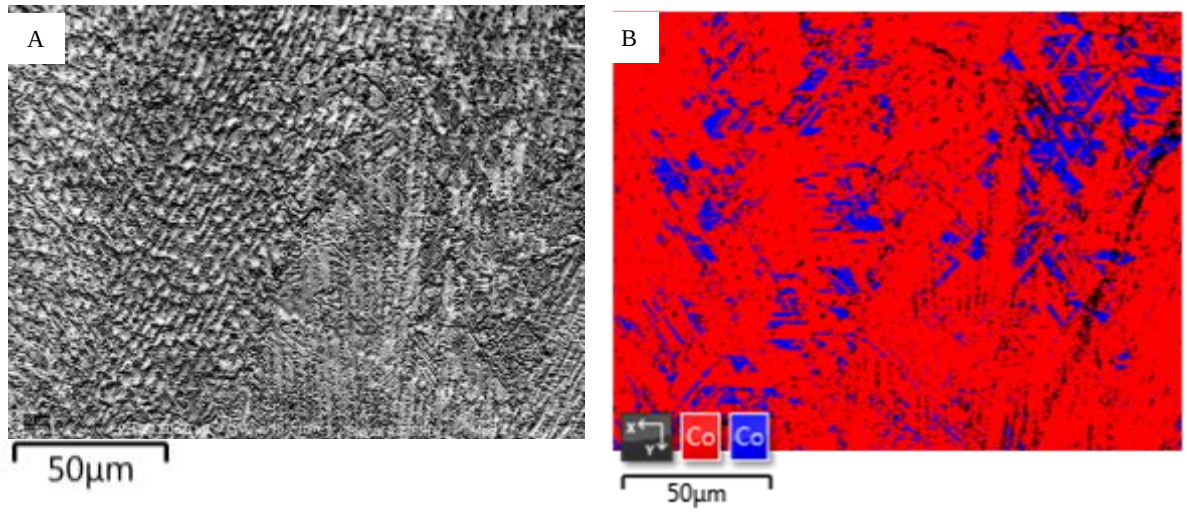

Figure 19 A) SEM image for 0.05 wt. % C as-built condition, B) Phase map of SEM image. Red colour: ε-hcp phase, Blue colour: γ-fcc phase

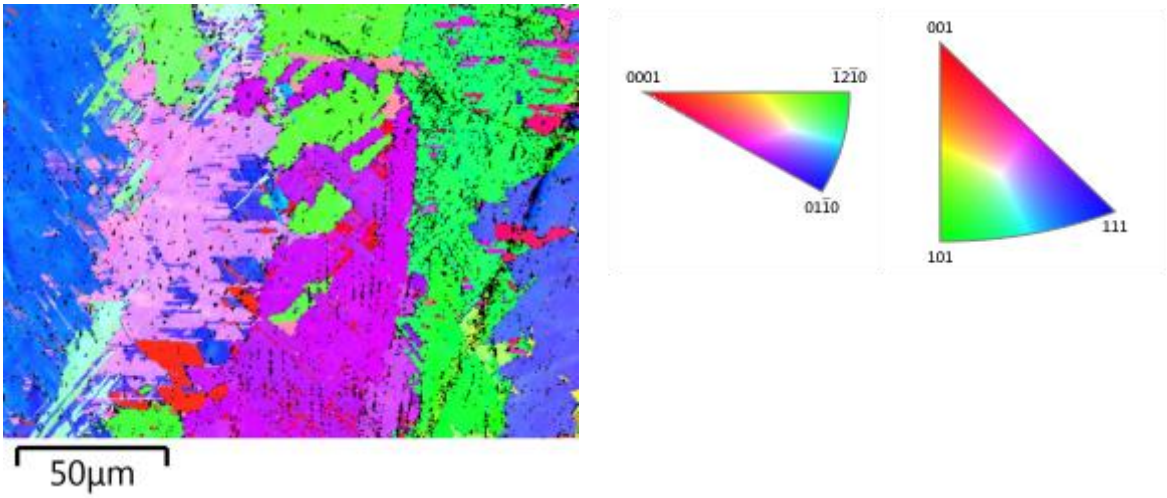

Figure 20 IPF map in z direction of SEM image in figure 19

Table 9 Phase distribution of 0.05 wt. % C as-built by EBSD analysis

Phase Name	Phase Fraction (%)	Phase Count	Mean MAD
Co-ε hcp (Red color)	82.09	91965	0.60
Co-γ fcc (Blue color)	11.61	13011	0.69
Zero Solutions (Black dots)	6.30	7059	

The phase map shows the phase distribution in the 0.05 wt.% C as-built condition. The above results confirm the two phases present as ε-hcp martensitic and γ-fcc phase with ε-hcp as the dominant phase at ~82.09%. These results overlap with phase quantification results obtained based on XRD peaks where the dominant ε-hcp phase fraction is ~88.7%. The zero solutions or in other words, no solutions during phase identification can be result of various factors. It

can be because of carbides, impurities picked up during sample preparation or electrolytic etching, grain boundaries etc.

Scan 2

The EBSD analysis was done on HIPed sample with 0.05 wt.% C on the horizontal cross section.

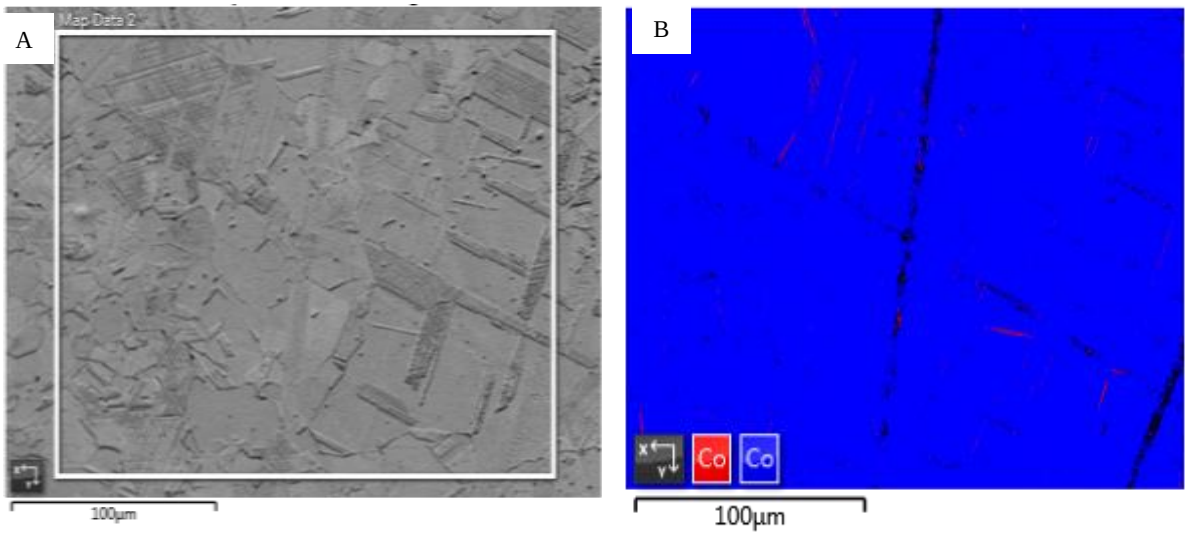

Figure 21 A) SEM image of 0.15 wt. % C HIP condition B) Phase map of SEM image. Red colour: ε-hcp phase, Blue colour: γ-fcc phase

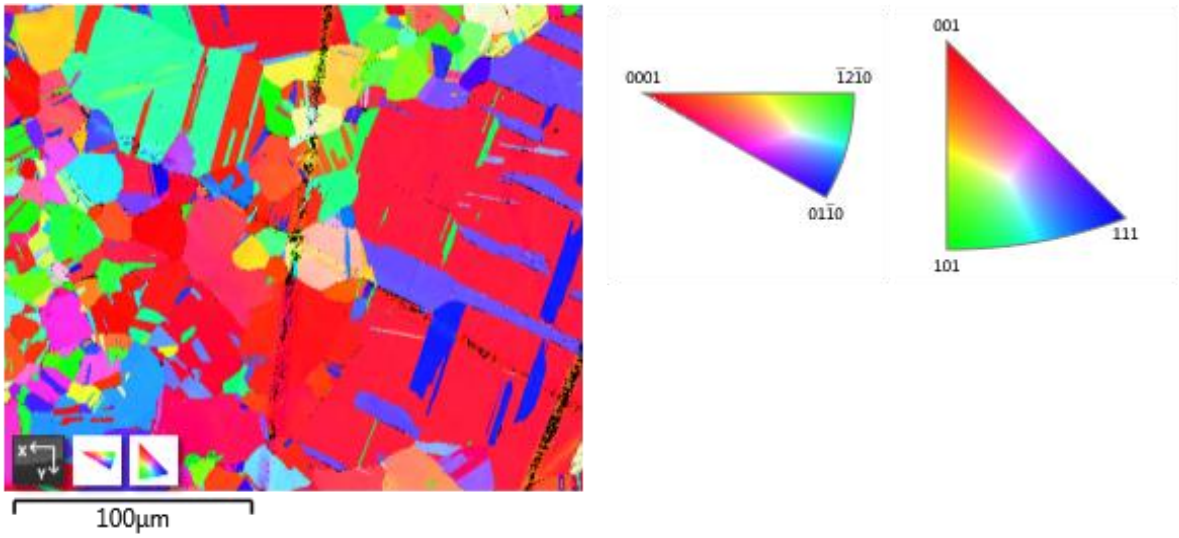

Figure 22 IPF map in z direction of SEM image in figure 21-A

Table 10 Phase distribution of 0.15 wt. % C by EBSD analysis

Phase Name	**Phase Fraction (%)**	**Phase Count**	**Mean MAD**
Co-ε hcp (Red color)	0.40	778	0.78
Co-γ fcc (Blue color)	98.10	189196	0.45
Zero Solutions (Black dots)	1.49	2878	

The phase map shows the phase distribution in the 0.05 wt.% C after HIP treatment. As compared to phase map for as-built state (figure 19-B), blue colour representing γ-fcc phase

dominates after HIPing. According to the phase quantification, the dominant phase matrix is γ-fcc with phase fraction reaching as high as 98.10 %. This can also be confirmed by XRD analysis where the γ-fcc phase fraction is 99.50%. The IPF map in z direction is indicative of grain orientation in z direction. Sharp contrast in color between grains is indicative that the grains are randomly distributed. Annealing twins can also be seen inside the grains. Grain size is inhomogeneous. This is because of recrystallization where new small grains are formed inside existing large grains. As can be seen in figure 12, complete recrystallization with uniform grain size has not achieved.

Observations

Hardness test

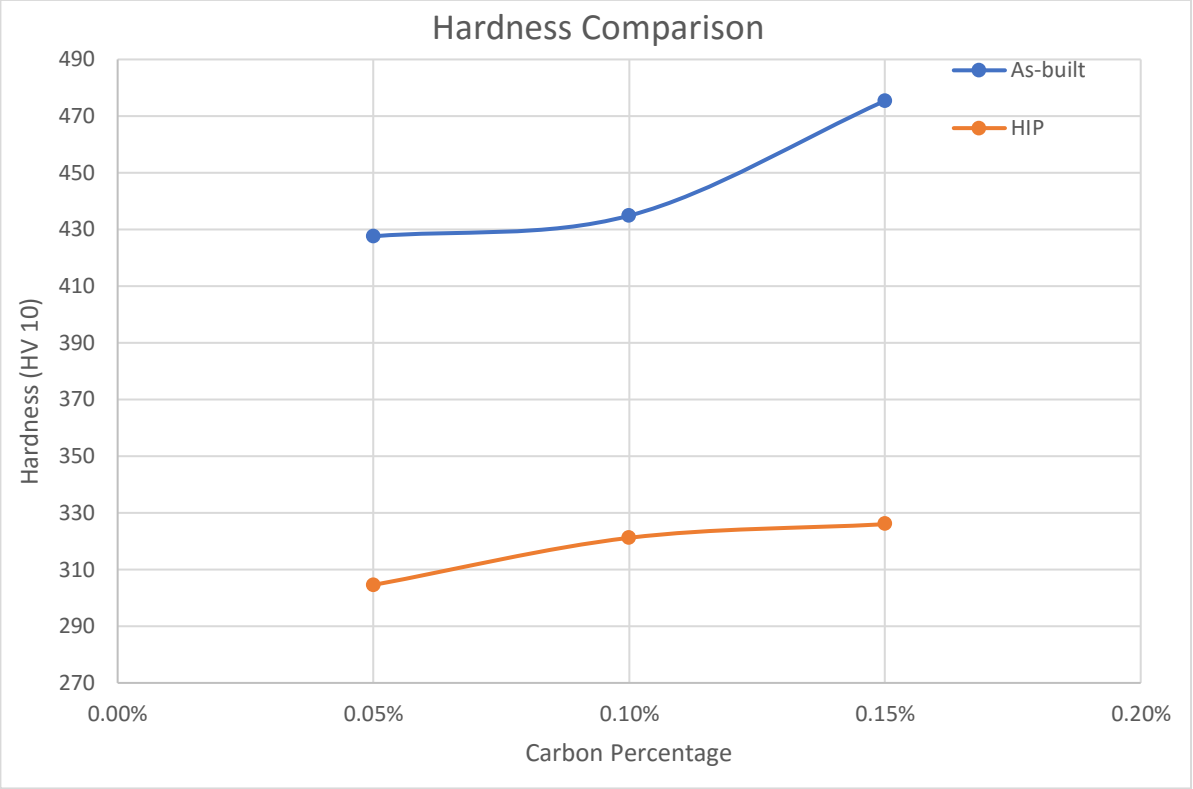

Figure 23 Micro-hardness results

The hardness of the as-built samples is higher than HIPed samples by 120-150 HV. This result indicates that γ-fcc phase after HIP treatment is softer than ε-hcp phase in as-built state. Additionally, the hardness increases with increasing C & N content in the alloy. This implies that precipitates help increase the hardness of the alloy.

Observations

Discussion

The observed microstructure and hardness test results were then compared to the corresponding mechanical tensile test result which were provided by Arcam EBM AB (attached in appendix-I). All the samples with varying carbon & nitrogen content in as-built and HIP condition were tested for two loading directions 1) Z direction parallel to build direction 2) XY direction perpendicular to build direction.

Looking at the YS results, all the as-built samples satisfy the minimum strength of 450 MPa as required by the ASTM F75 standard. For HIPed samples, 0.05 wt.% C XY direction sample has the lowest strength and just satisfies the 450 MPa criteria with average strength of 468 MPa. On comparing the YS of as-built and HIP samples, there is relatively larger difference between two loading directions for as-built samples than for HIPed samples. This may be because of the columnar grains and cylindrical carbide microstructure of as-built samples as compared to equi-axed grains and globular carbides microstructure of HIPed samples. Different grains size in different direction results in anisotropic property of as-built samples while HIPed samples show isotropic strength. There is a slight decrease in overall YS after HIPing relative to corresponding as-built samples. This may be because of the different dominant phases present. By looking at the phase analysis results and hardness values, HIPed samples have a softer γ-fcc dominant phase and as-built samples have more brittle and harder ε-hcp dominant phase. The brittle ε-hcp phase with fewer slip system results in higher YS for as-built samples. For as-built condition, 0.1 and 0.15 wt. % C XY direction samples have higher YS than in Z direction. After HIPing, 0.1 wt. % C shows the highest YS.

All the samples in as-built and HIP condition satisfy the minimum ultimate tensile strength (UTS) requirement of 655 MPa. After HIPing, 0.05 wt. % C shows the highest UTS.

Looking at the elongation property results, all the as-built samples are below the 8 % elongation ASTM F75 criteria. On the contrary, elongation percentage for the corresponding HIPed samples increases by 2-3 times and are above 8 %. The primary reason again can be the dominant phase difference. As explained in literature study, ε-hcp dominant phase in as-built samples are characterized by brittle nature and low elongation property while γ-fcc dominant phase after HIPing are characterized by their high elongation property. After HIPing, the elongation decreases with increasing C content with highest elongation percentage for 0.05 wt. % C. This can be because of the increasing carbide precipitate concentration at grain boundary with increasing C content. As can be seen in SEM images for HIPed samples (figure 15), 0.05 wt. % C shows no cavities at grain boundaries but cavity concentration at grain boundary increases for 0.10 and 0.15 wt. % C. The cavities are assumed to be precipitate sites which are etched away during electrolytic etching or sample preparation procedure. The precipitates at grain boundaries may act as sites of stress concentration and crack nucleation leading to reduced elongation percentage.

Discussion

Summary

	As-built	HIP
Orientation	• Anisotropic, columnar grains along build direction	• Isotropic, equi-axed grains
Phase	• ε-hcp, brittle, poor elongation	• γ-fcc, higher elongation
Precipitates	• Cylindrical precipitates • With increasing C %, precipitates at grain boundary	• Partial dissolution • Globular precipitates • With increasing C %, precipitates at grain boundary
Hardness	• 430-470 HV	• 300-325 HV
YS	• Higher relative to HIP condition	• Maximum for 0.1 wt.% C
Elongation	• Below 8%	• Above 8% • Decreases with increasing carbon content

Summary

Conclusion

For biomedical applications, it is very important that the implants are defect free and comply to the standards set by the medical community. As a result, detailed quality checks are done for implants strength and durability. This thesis work has indicated that cubical samples made by EBM technique using the CCM-CN alloy have anisotropic microstructure and mechanical strength. The samples have cylindrical precipitates along build direction and ε-hcp dominant phase matrix which shows poor elongation (below 8% minimum requirement set by ASTM F75 standard) and brittle fracture. After the samples are heat treated (HIP), isotropic microstructure and mechanical strength are obtained. The samples have globular precipitates and γ-fcc dominant phase matrix which shows high elongation (above 8%). These results indicate that HIP treatment improves the elongation of as-built samples by recrystallization, phase change and partial dissolution of precipitates. HIP is also important in removing defects introduced during additive manufacturing like pores and cracks.

For parts made using investment casting and hot forging process, the optimum concentration of C and N lies in the range 0.05-0.10 wt.% and 0.15-0.22 wt.% respectively. These trace elements are added with the aim of stabilizing γ-fcc phase relative to ε-hcp phase during solidification process and to increase elongation, YS and UTS. However, these C and N do not have the same beneficiary effects for parts made using EBM technique without HIP treatment. The elongation for as-built samples with C and N content between (0.05-0.15 wt.%) is below 8% minimum requirement by ASTM F75 standard. Moreover, the C and N added with the aim of stabilizing γ-fcc phase relative to ε-hcp phase is not suitable for EBM technique because of the high sintering temperature used. The build is held at temperatures between 600-800°C for 25-30 hours (based on build size and shape) which corresponds to ε-hcp phase region in the phase diagram. As a result, the metastable γ-fcc transforms to stable ε-hcp phase during prolonged heating. Moreover, increasing C and N content up to 0.15 wt.% is not beneficial for elongation property after HIP treatment. With increasing concentration of trace elements, it leads to increasing concentration of precipitates at grain boundaries which decreases the elongation percentage. Hence, C and N should be added to a weight percentage that provides solid solution and precipitation strengthening effect without compromising the elongation property after HIP treatment.

CCM-0.10C-0.09N shows the best mechanical tensile property after HIP treatment among the samples tested.

Conclusion

Suggested future work

- Fracture surface characterization of tensile test samples.
- Study on deformation mechanisms active during straining and correlate it to fracture surface characteristics.
- Perform microstructural characterization and mechanical testing of as-built and HIP samples consisting of low C (max. 0.05 wt.%) and increasing N (max. 0.25 wt.%) to understand the effect of individual trace elements. N addition results in formation of nano nitrides which have very good strengthening effect. Solubility of N increases without C.
- The hardness of the CCM alloy samples decreases after HIP treatment. This may have negative effects on wear resistance and the ability to form mirror finish implants. Hence, HIP cycle can be optimized to improve hardness.
- More literature study on the effect of other trace elements like silicon, zirconium.

Suggested future work

References

[1] ASTM, “Standard Terminology for Additive Manufacturing Technologies,” pp. 2–4, 2011.

[2] R. Singh, S. Singh, and M. Hashmi, “Implant Materials and Their Processing Technologies,” in *Reference Module in Materials Science and Materials Engineering*, Elsevier, 2016, pp. 1–31.

[3] W. J. Sames, F. A. List, S. Pannala, R. R. Dehoff, and S. S. Babu, “The metallurgy and processing science of metal additive manufacturing,” *Int. Mater. Rev.*, vol. 6608, no. March, pp. 1–46, 2016.

[4] S. H. Huang, P. Liu, A. Mokasdar, and L. Hou, “Additive manufacturing and its societal impact: A literature review,” *Int. J. Adv. Manuf. Technol.*, vol. 67, no. 5–8, pp. 1191–1203, 2013.

[5] L. E. Murr, “Metallurgy of additive manufacturing: Examples from electron beam melting,” *Addit. Manuf.*, vol. 5, pp. 40–53, 2015.

[6] ASTM International, “F2792-12a - Standard Terminology for Additive Manufacturing Technologies,” *Rapid Manuf. Assoc.*, pp. 10–12, 2013.

[7] S. H. Sun, Y. Koizumi, S. Kurosu, Y. P. Li, and A. Chiba, “Phase and grain size inhomogeneity and their influences on creep behavior of Co-Cr-Mo alloy additive manufactured by electron beam melting,” *Acta Mater.*, vol. 86, pp. 305–318, 2015.

[8] Arcam EBM AB, “Arcam Brochure – the innovative leader in additive manufacturing solutions for the production of orthopedic implants and aerospace components.,” p. 19, 2016.

[9] L. E. Murr, S. M. Gaytan, E. Martinez, F. Medina, and R. B. Wicker, “Next generation orthopaedic implants by additive manufacturing using electron beam melting,” *Int. J. Biomater.*, vol. 2012, 2012.

[10] J. Hiemenz, “Electron beam melting,” *Adv. Mater. Process.*, vol. 165, no. 3, pp. 45–46, 2007.

[11] C. Requirements, O. S. Iron, C. Alloys, H. R. Steels, H. Steels, and I. Alloys, “Astm F75,” pp. 1–4, 2014.

[12] S. Boedo and S. A. Coots, “Wear Characteristics of Conventional and Squeeze-Film Artificial Hip Joints,” *J. Tribol.*, vol. 139, no. 3, p. 31603, 2016.

[13] K. Yamanaka, M. Mori, and A. Chiba, “Effects of nitrogen addition on microstructure and mechanical behavior of biomedical Co-Cr-Mo alloys,” *J. Mech. Behav. Biomed. Mater.*, vol. 29, pp. 417–426, 2014.

[14] S. H. Sun, Y. Koizumi, S. Kurosu, Y. P. Li, H. Matsumoto, and A. Chiba, “Build direction dependence of microstructure and high-temperature tensile property of Co-Cr-Mo alloy fabricated by electron beam melting,” *Acta Mater.*, vol. 64, pp. 154–168, 2014.

[15] S. M. Gaytan *et al.*, “Comparison of microstructures and mechanical properties for solid and mesh cobalt-base alloy prototypes fabricated by electron beam melting,” *Metall. Mater. Trans. A Phys. Metall. Mater. Sci.*, vol. 41, no. 12, pp. 3216–3227, 2010.

[16] Arcam EBM AB, “Arcam ASTM F75 CoCr Brochure.”

[17] K. Yoda *et al.*, “Effects of chromium and nitrogen content on the microstructures and mechanical properties of as-cast Co-Cr-Mo alloys for dental applications,” *Acta Biomater.*, vol. 8, no. 7, pp. 2856–2862, 2012.

[18] S.-H. SUN, Y. KOIZUMI, S. KUROSU, Y.-P. LI, and A. CHIBA, “Effect of Phase Transformation on Tensile Behavior of Co-Cr-Mo Alloy Fabricated by Electron-beam Melting,” *J. Japan Soc. Powder Powder Metall.*, vol. 61, no. 5, pp. 234–242, 2014.

[19] S.-H. Lee, N. Nomura, and A. Chiba, “Significant Improvement in Mechanical

Properties of Biomedical Co-Cr-Mo Alloys with Combination of N Addition and Cr-Enrichment," *Mater. Trans.*, vol. 49, no. 2, pp. 260–264, 2008.
[20] Y. Li *et al.*, "Influence of carbon and nitrogen addition on microstructure and hot deformation behavior of biomedical Co-Cr-Mo alloy," *Mater. Chem. Phys.*, vol. 135, no. 2–3, pp. 849–854, 2012.
[21] ASM, *Metallography and Microstructure*. ASM International, 2004.
[22] T. O. S. U. Hirth John Price (Department of Metallurgical Engineering and O. U. Lothe Jens (Institute of Physics, *Theory of dislocations*. McGRAW-HILL BOOL COMPANY.
[23] M. Mori, K. Yamanaka, K. Kuramoto, K. Ohmura, T. Ashino, and A. Chiba, "Effect of carbon on the microstructure, mechanical properties and metal ion release of Ni-free Co-Cr-Mo alloys containing nitrogen," *Mater. Sci. Eng. C*, vol. 55, pp. 145–154, 2015.
[24] R. V. Marrey, R. Burgermeister, R. B. Grishaber, and R. O. Ritchie, "Fatigue and life prediction for cobalt-chromium stents: A fracture mechanics analysis," *Biomaterials*, vol. 27, no. 9, pp. 1988–2000, 2006.
[25] A. Nagai, Y. Tsutsumi, Y. Suzuki, K. Katayama, T. Hanawa, and K. Yamashita, "Characterization of air-formed surface oxide film on a Co-Ni-Cr-Mo alloy (MP35N) and its change in Hanks' solution," *Appl. Surf. Sci.*, vol. 258, no. 14, pp. 5490–5498, 2012.
[26] T. Kilner, A. J. Dempsey, R. M. Pilliar, and G. C. Weatherly, "The effects of nitrogen additions to a cobalt-chromium surgical implant alloy," *J. Mater. Sci.*, vol. 22, no. 2, pp. 565–574, Feb. 1987.
[27] Y. P. Li, J. S. Yu, S. Kurosu, Y. Koizumi, H. Matsumoto, and A. Chiba, "Role of nitrogen addition in stabilizing the gamma phase of Biomedical Co-29Cr-6Mo alloy," *Mater. Chem. Phys.*, vol. 133, no. 1, pp. 29–32, 2012.
[28] S.-H. Lee, E. Takahashi, N. Nomura, and A. Chiba, "Effect of Carbon Addition on Microstructure and Mechanical Properties of a Wrought Co–Cr–Mo Implant Alloy," *Mater. Trans.*, vol. 47, no. 2, pp. 287–290, 2006.
[29] H. Matsumoto, S. Kurosu, B. S. Lee, Y. Li, and A. Chiba, "Deformation mode in biomedical Co-27% Cr-5% Mo alloy consisting of a single hexagonal close-packed structure," *Scr. Mater.*, vol. 63, no. 11, pp. 1092–1095, 2010.
[30] H. Matsumoto, S. Kurosu, B. S. Lee, Y. Li, Y. Koizumi, and A. Chiba, "Deformation behavior of biomedical Co-Cr-Mo alloy," *Miner. Met. Mater. Soc.*, vol. 3, pp. 433–437, 2011.
[31] B. S. Lee, H. Matsumoto, and A. Chiba, "Fractures in tensile deformation of biomedical Co-Cr-Mo-N alloys," *Mater. Lett.*, vol. 65, no. 5, pp. 843–846, 2011.
[32] A. Mani, Salinas-Rodriguez, and H. F. Lopez, "Deformation induced FCC to HCP transformation in a Co-27Cr-5Mo-0.05C alloy," *Mater. Sci. Eng. A*, vol. 528, no. 7–8, pp. 3037–3043, 2011.
[33] R. Kaiser, K. Williamson, and C. O'Brien, "Effects of hot isostatic pressing and heat treatment on cast cobalt alloy," *Mater. Sci.*, vol. 31, no. 11, pp. 1298–1304, 2015.
[34] A. G. Bowles and D. E. Witkin, "Hot Isostatic Pressing," *High-Pressure Sci. Technol.*, pp. 1718–1726, 1979.
[35] D. Richter, G. Haour, and D. Richon, "Hot isostatic pressing (HIP)," *Mater. Des.*, vol. 6, no. 6, pp. 303–305, 1985.
[36] R. Widmer, *Hot Isostatic Pressing in Competition and in Combination With Other Consolidation Processes*. Elsevier Science B.V., 1994.
[37] R. Kircher, a Christensen, and K. Wurth, "Electron Beam Melted (EBM) Co-Cr-Mo Alloy for Orthopaedic Implant Applications R.S. Kircher, A.M. Christensen, K.W. Wurth Medical Modeling, Inc., Golden, CO 80401," *Solid Free. Fabr. Proc.*, pp. 428–

436, 2009.
[38] Unknown, “Etching Specialty Alloys,” no. February, pp. 1–6, 2008.
[39] S. Practice, “Standard Practice for Microetching Metals and Alloys ASTM E-407,” vol. 7, no. Reapproved 2015, pp. 1–22, 2016.
[40] Oxford Instruments, “EBSD Electron Backscatter Diffraction.”
[41] R. Jenkins and R. Snyder, “Quantitative Analysis,” in *Introduction to X-ray Powder Diffractometry*, Hoboken, NJ, USA: John Wiley & Sons, Inc., 2012, pp. 355–387.
[42] ASTM E92-16., “Standard Test Methods for Vickers Hardness and Knoop Hardness of Metallic Materials,” *Am. Soc. Test. Mater.*, vol. 82, no. July 2010, pp. 1–27, 2016.

References

Appendix I, Tensile test results

The tensile test was performed for 2 directions. 1) Z direction parallel to build direction 2) XY direction perpendicular to build direction.

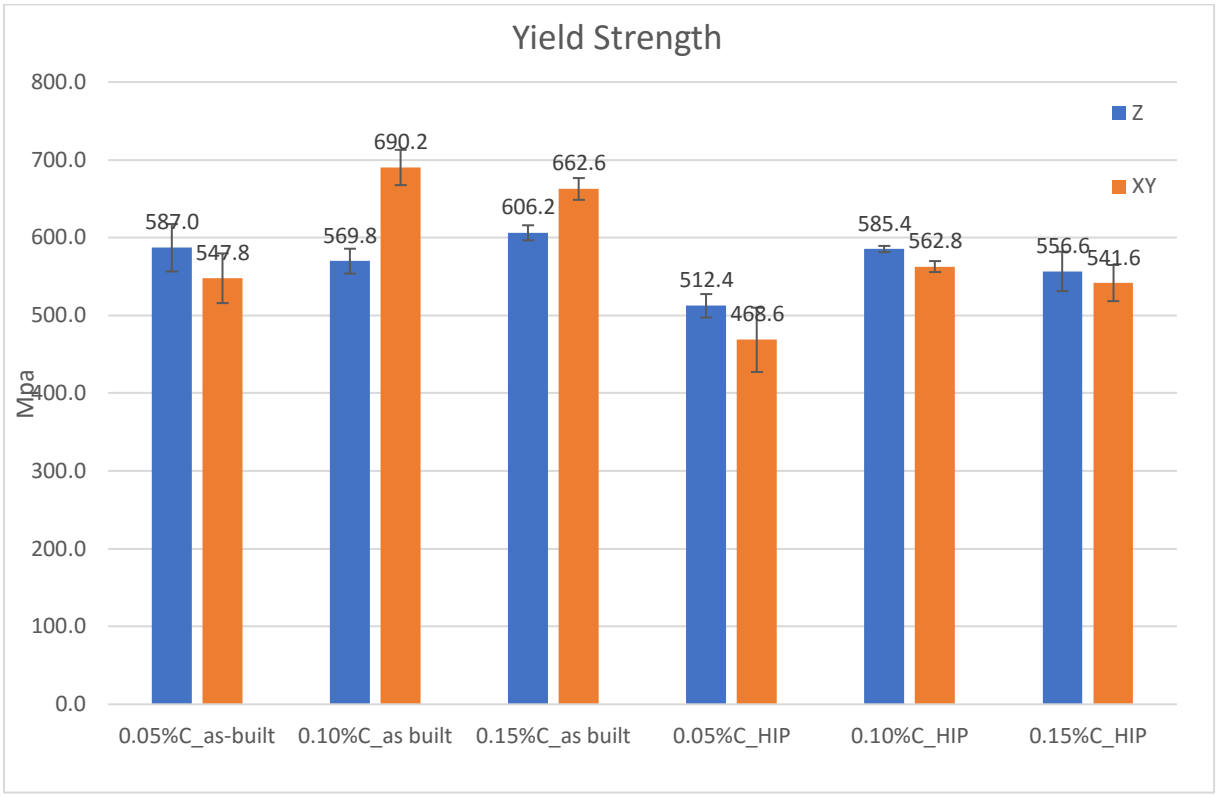

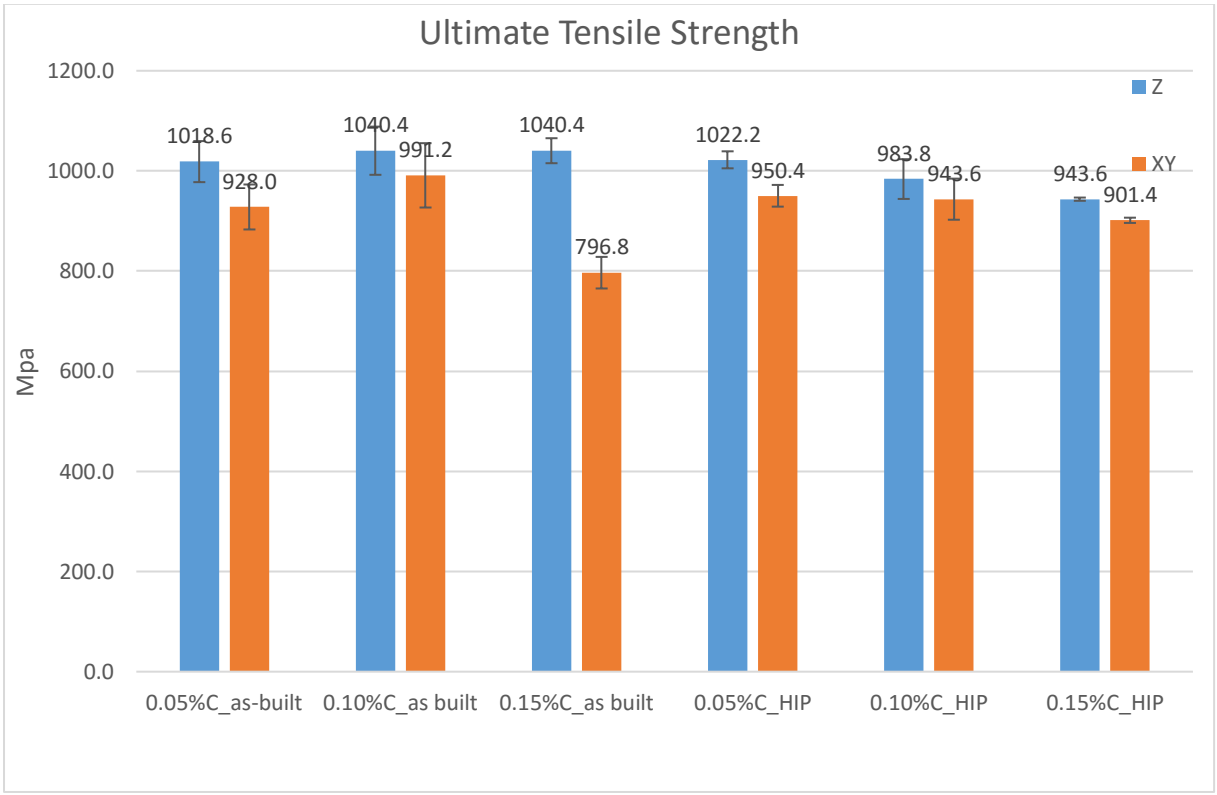

Appendix I, Tensile test results

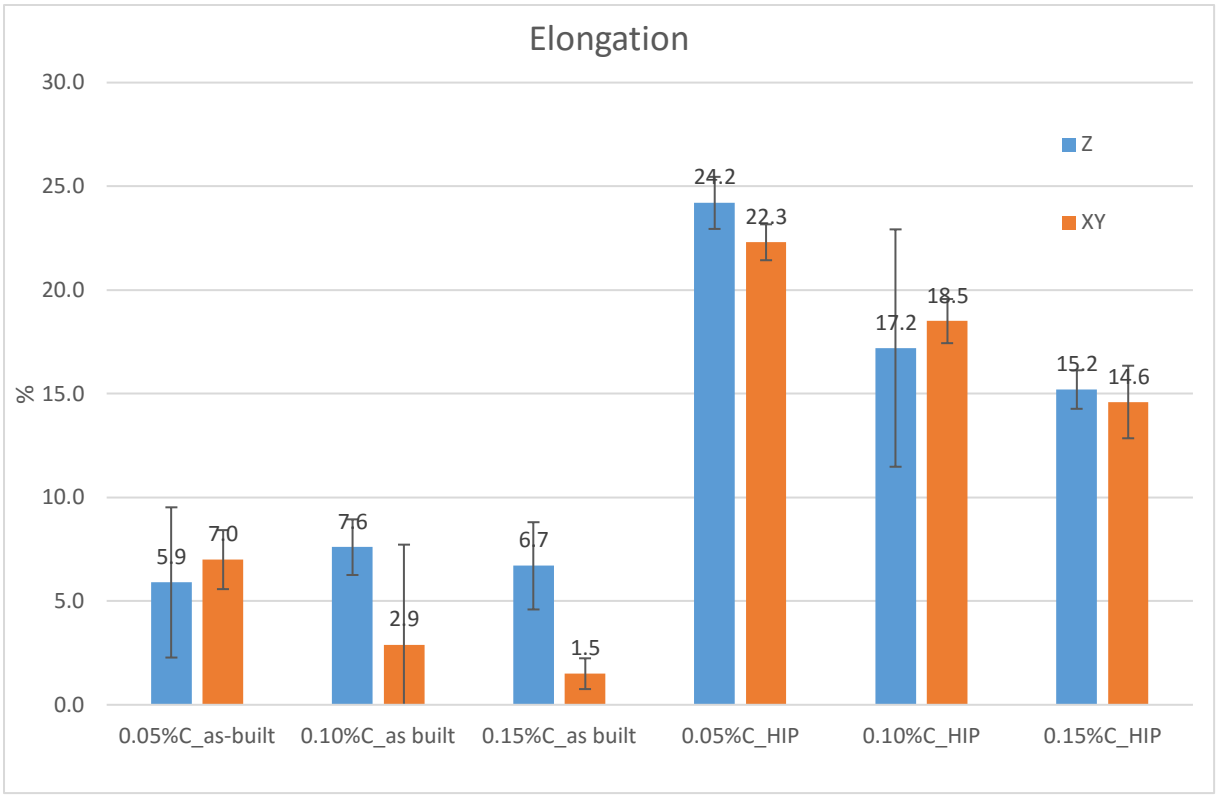

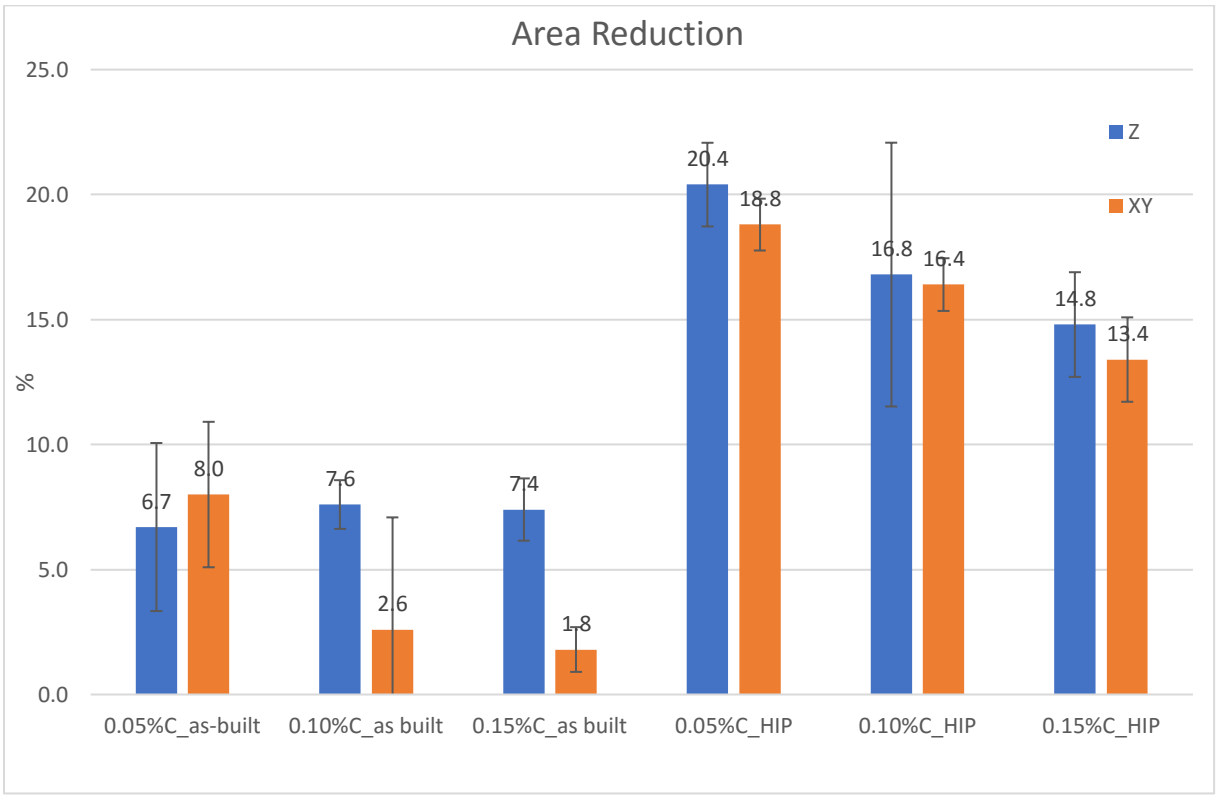

Appendix II, Microstructural images

As-built, 0.05 wt. % C

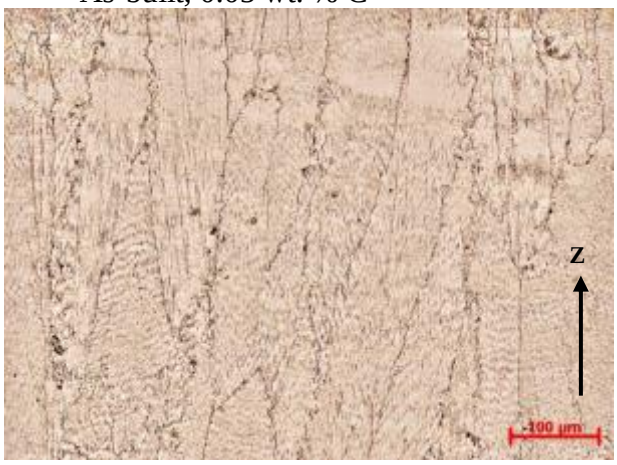

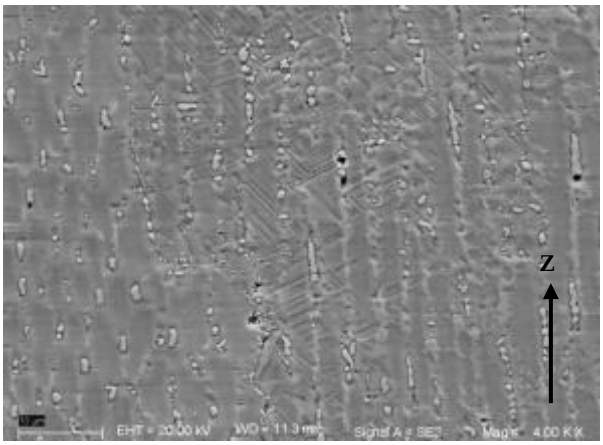

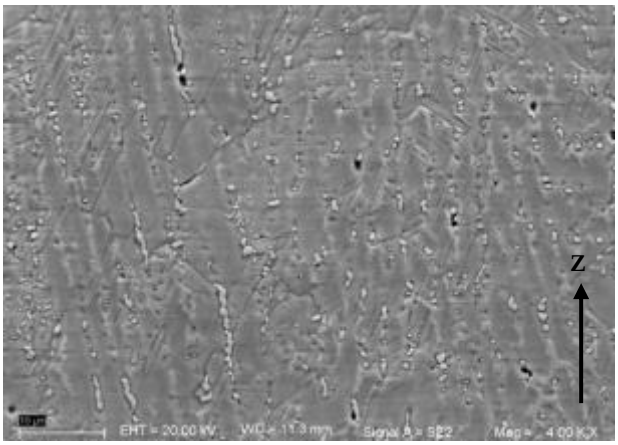

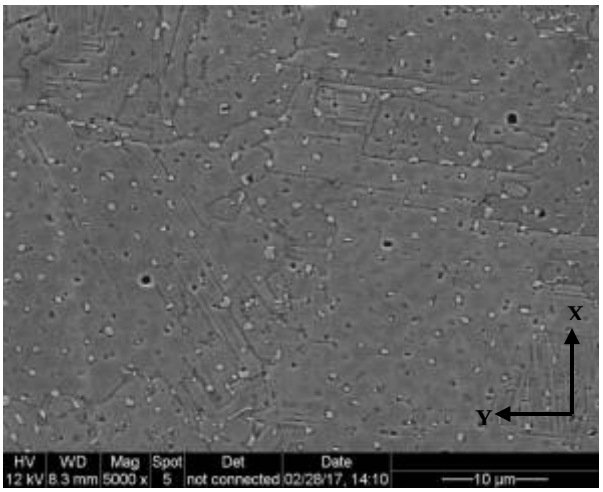

Appendix II, Microstructural images

HIP, 0.05 wt. % C

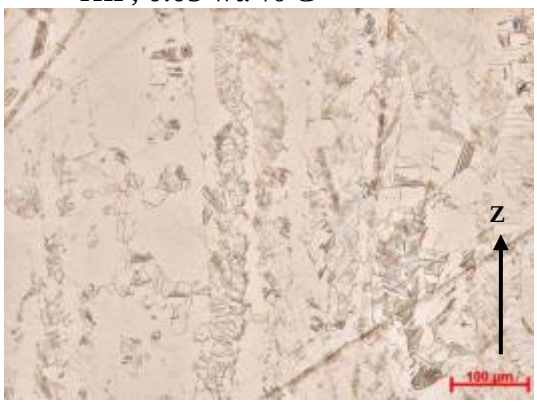

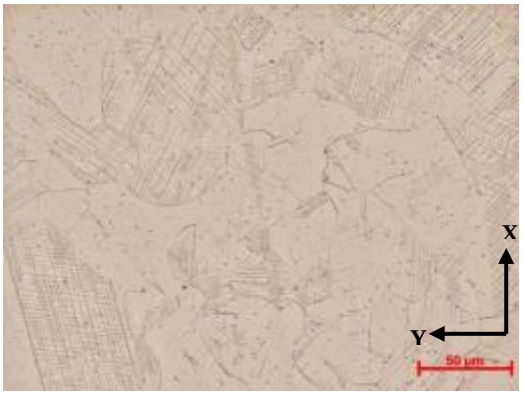

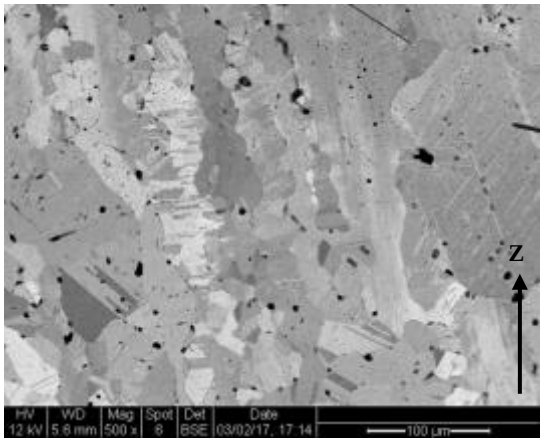

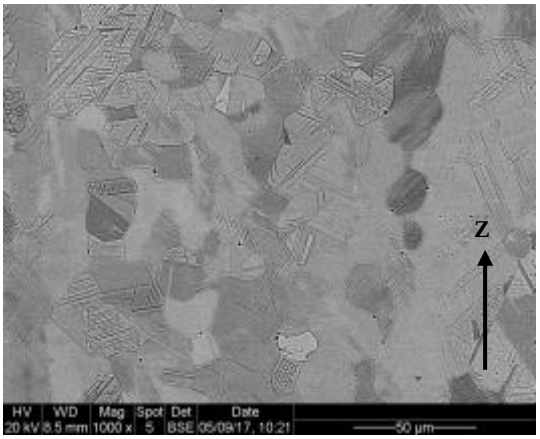

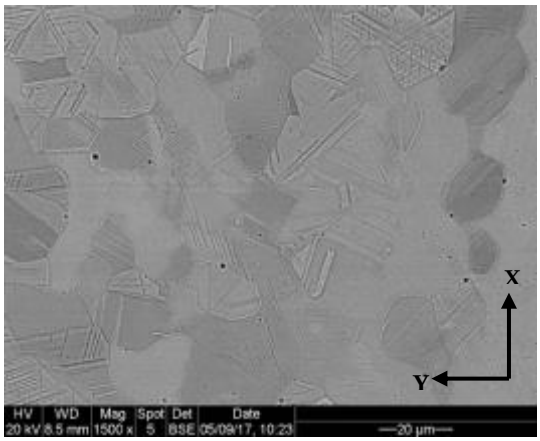

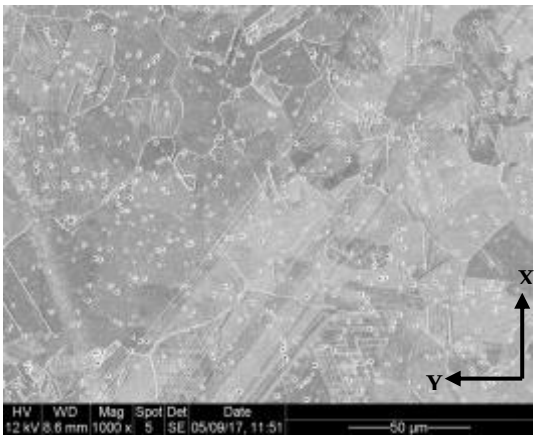

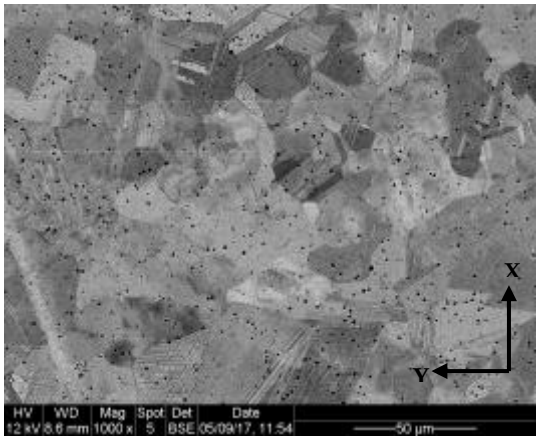

As-built, 0.10 wt. % C

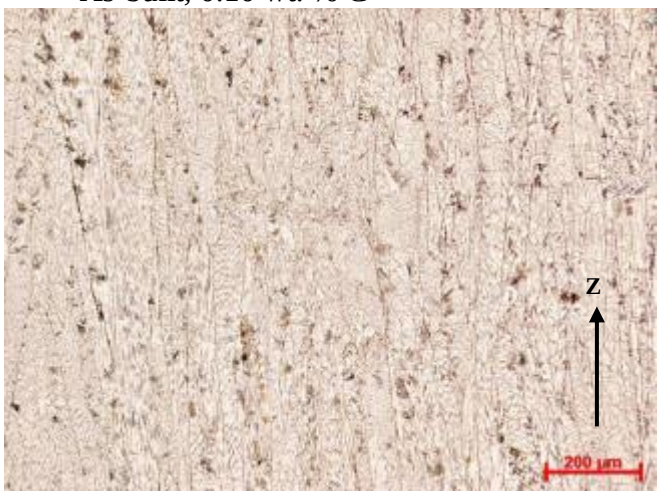

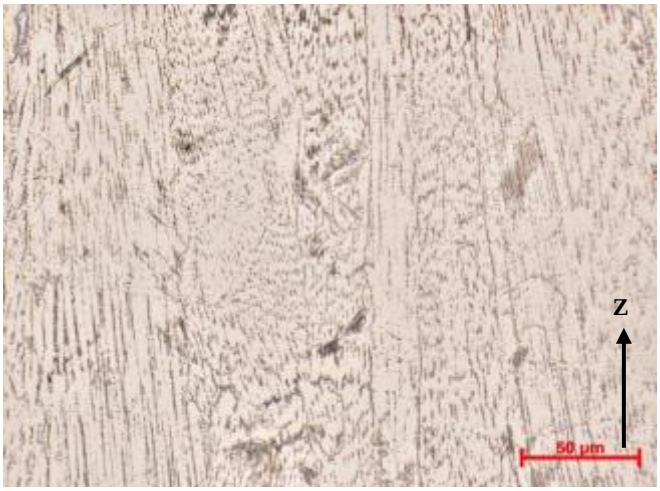

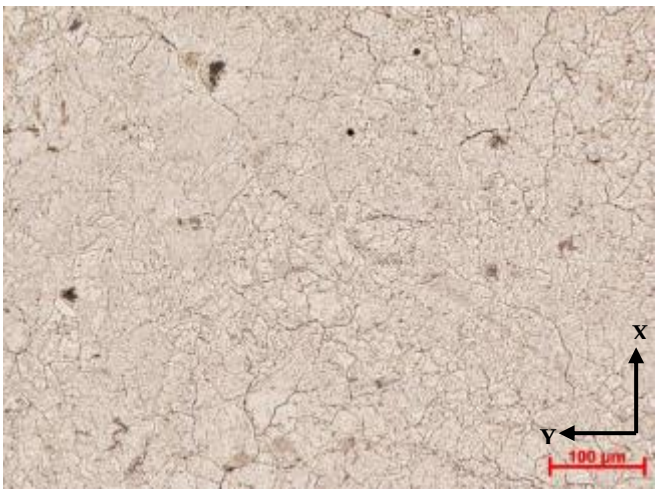

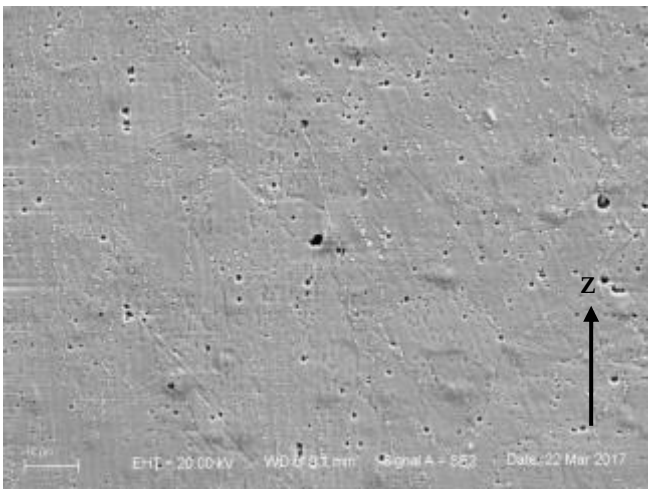

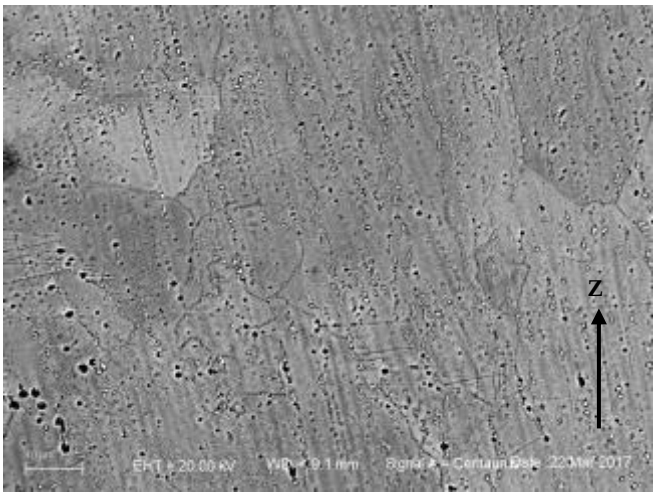

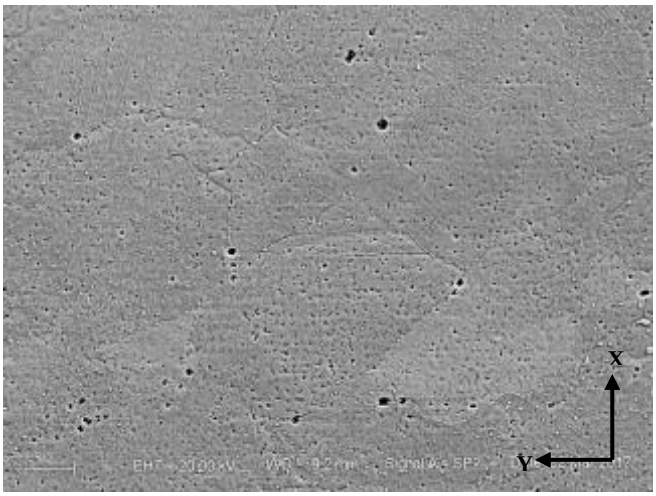

Appendix II, Microstructural images

HIP, 0.10 wt.% C

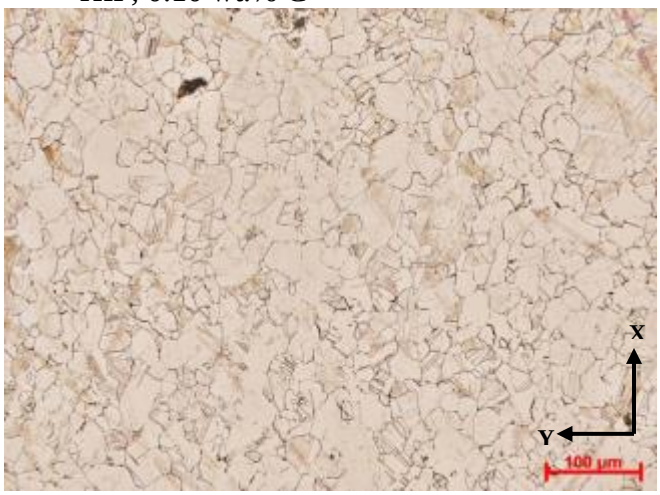

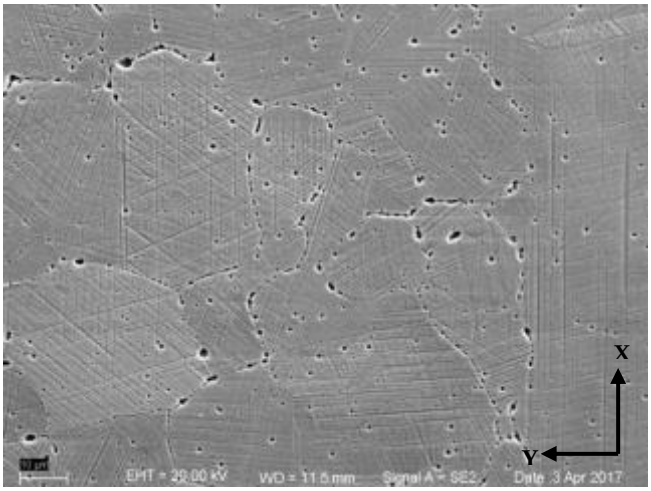

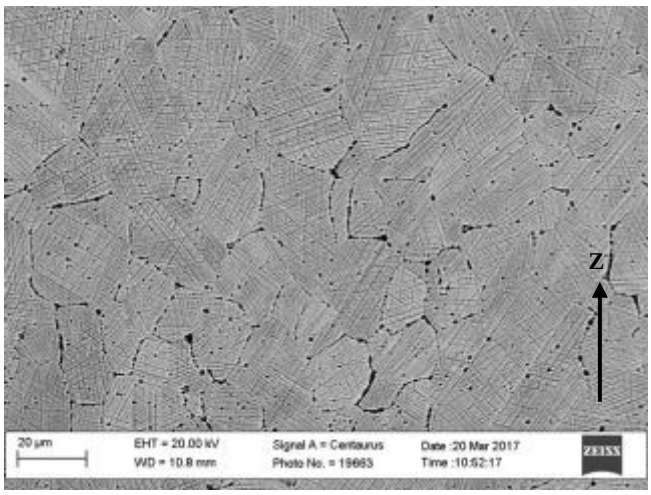

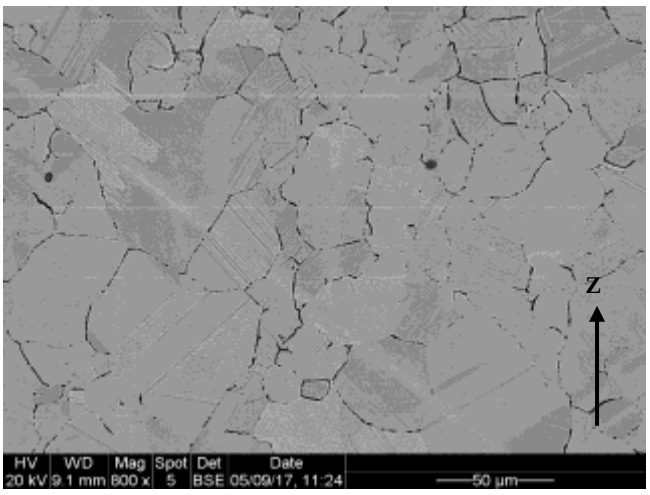

As-built, 0.15 wt. % C

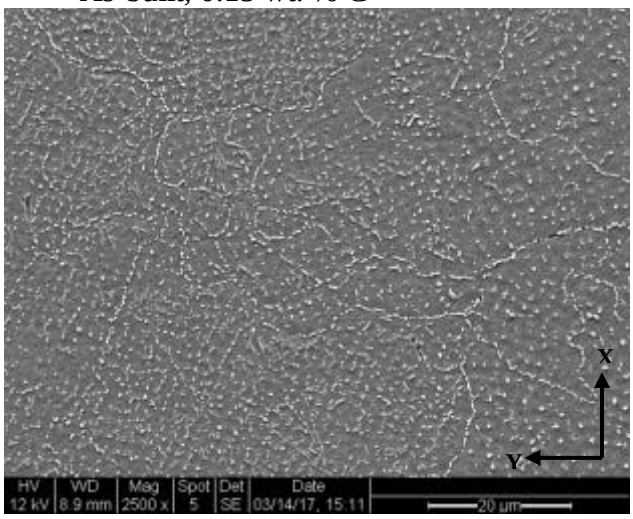

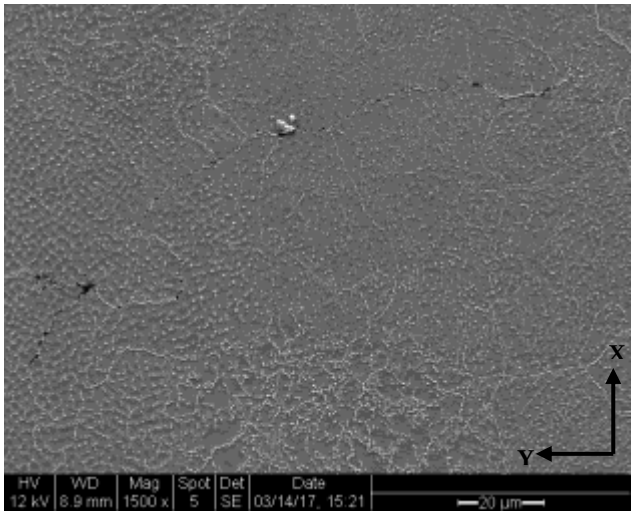

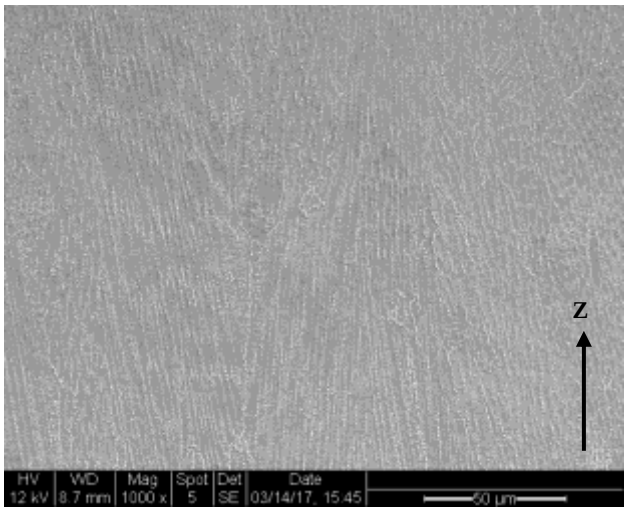

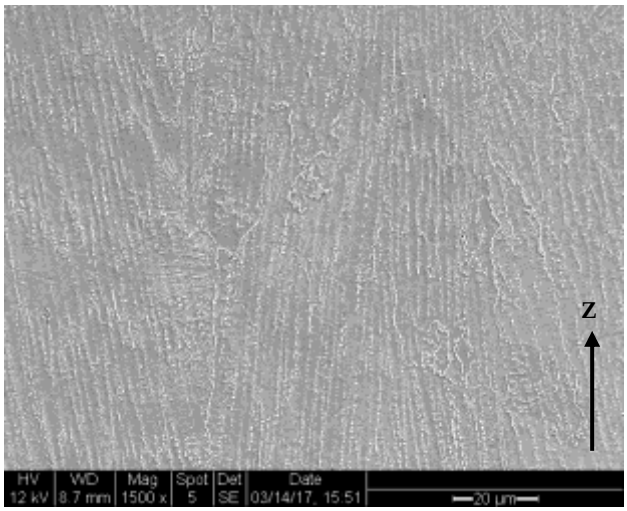

Appendix II, Microstructural images

HIP, 0.15 wt. % C